Comput Mech (2014) 53:413–435
DOI 10.1007/s00466-013-0962-4

REVIEW PAPER

Encapsulated microbubbles and echogenic liposomes for contrast ultrasound imaging and targeted drug delivery

Shirshendu Paul · Rahul Nahire · Sanku Mallik · Kausik Sarkar

Received: 20 July 2013 / Accepted: 10 December 2013 / Published online: 3 January 2014

Abstract Micron- to nanometer-sized ultrasound agents, like encapsulated microbubbles and echogenic liposomes, are being developed for diagnostic imaging and ultrasound mediated drug/gene delivery. This review provides an overview of the current state of the art of the mathematical models of the acoustic behavior of ultrasound contrast microbubbles. We also present a review of the in vitro experimental characterization of the acoustic properties of microbubble based contrast agents undertaken in our laboratory. The hierarchical two-pronged approach of modeling contrast agents we developed is demonstrated for a lipid coated (Sonazoid^{TM}) and a polymer shelled (poly D- L-lactic acid) contrast microbubbles. The acoustic and drug release properties of the newly developed echogenic liposomes are discussed for their use as simultaneous imaging and drug/gene delivery agents. Although echogenicity is conclusively demonstrated in experiments, its physical mechanisms remain uncertain. Addressing questions raised here will accelerate further development and eventual clinical approval of these novel technologies.

Keywords Ultrasound contrast agents · Encapsulated microbubbles · Liposomes · Drug delivery

S. Paul
Department of Mechanical Engineering, University of Delaware, Newark, DE 19716, USA

R. Nahire · S. Mallik
Department of Pharmaceutical Sciences, North Dakota State University, Fargo, ND 58108, USA

K. Sarkar (✉)
Department of Mechanical and Aerospace Engineering, The George Washington University, Washington, DC 20052, USA
e-mail: Sarkar@gwu.edu

1 Introduction

In recent years, a number of innovative particulate systems—nanoparticles [1], nanoemulsions [2], quantum dots [3], 'bubbicles' [4], vesicles and microbubbles—are being developed for healthcare applications. They are aimed at the dual purpose of early accurate diagnosis of diseases—as contrast enhancing agents for medical imaging—and their rapid remediation—as delivery vehicles for therapeutic agents. The effectiveness of these agents critically depends on our ability to engineer them using sound physical principles. Here, we will present an overview of the ongoing research in our laboratory on the analysis and characterization of encapsulated microbubbles and acoustically active echogenic liposomes (ELIP) for contrast enhanced ultrasound (CEUS) imaging and drug delivery.

Microbubble based ultrasound contrast agents (UCA) has been approved by the federal Food and Drug Administration (FDA) for echocardiography. Echocardiography is one of the primary tools for diagnosing cardiovascular diseases—the leading cause of mortality in the US. However, more than 15 % of echocardiographs in the US are suboptimal, i.e. they do not result in definitive diagnosis [5,6]. UCA can substantially improve the diagnostic abilities of not only echocardiography but also of ultrasound of liver, kidney and other organs [7–9]. On the other hand, of all the particulates, liposomes are a prime candidate for drug delivery because of their structural similarities with biological cells, long circulation times and ability to carry both hydrophobic [10] and hydrophilic [11,12] drugs. ELIP combine these advantages of liposomes with the echogenicity or ultrasound responsiveness of microbubbles, making them an excellent candidate for concurrent ultrasound imaging and drug delivery.

We have been studying the dynamics of these contrast and drug delivery agents through both in vitro experiments

and mathematical modeling. Our aim is to develop reliable tools for characterizing their behaviors that can be used to design and develop the next generation contrast and drug delivery agents. This paper presents an overview of the ongoing research on acoustic characterization of several commercial and experimental microbubble based contrast agents and ELIP. Section 2 presents a broad review of the state of the art of contrast agent applications. In Sect. 3, we briefly discuss the mathematical models to describe the behavior of microbubble based contrast agents including various interfacial rheological models of contrast agent encapsulation. In Sect. 4, we discuss the experimental approaches to characterize the acoustic behaviors of contrast microbubbles. In Sect. 5, we review the experimental results characterizing both the acoustic and drug release properties of ELIP. Both Sects. 4 and 5 provide some specific illustrative examples for clarifying key results and their implications. The final section summarizes the findings and discusses the scope of possible future research.

2 Background of contrast agent applications

Diagnostic medical imaging involves various modalities, viz., computed tomography, magnetic resonance imaging, ultrasound imaging etc. Although diagnostic imaging with ultrasound offers a safe, portable, low cost alternative, its applicability is often limited by inferior image quality and lack of spatial resolution in comparison to CT or MRI [7]. However, recent technological advances in the field of ultrasonics coupled with the rapid development of novel ultrasound contrast agents have led the medical community to investigate CEUS imaging for diagnosis of various cardiovascular, hepatic, renal, gastrointestinal and pancreatic diseases [7–9].

The poor scattering properties of human blood are a cause of non-definitive ultrasound images. A major breakthrough in this regard was the accidental discovery of the effectiveness of micron sized gas bubbles in enhancing ultrasound image contrast [13]. Due to the presence of the highly compressible gaseous core, these microbubbles can significantly enhance the backscatter of incident ultrasound waves through 'active scattering' [14]. For micron-sized bubbles, this active scattering cross-section is often several orders of magnitude higher than the 'passive scattering' cross-section (passive scattering is the primary source of scattered echo from tissues and blood). However, the potential for clinical applications of such uncoated microbubbles was severely restricted by their highly unstable nature. The pressure inside a gas bubble is higher than the outside pressure due to the surface tension forces at the air–water interface. This results in their rapid dissolution—in milliseconds for micron sized air bubble at room temperature [15,16]. To stabilize these gas bubbles against dissolution, microbubbles are encapsulated with a layer of lipid/protein/surfactant/polymer molecules [17]. Most commercially available and experimental contrast agents are 1–10 μm in diameter with a low solubility gas (viz., perfluorocarbons, and sulfur hexafluoride) inside and is stabilized with such an outer coating [17].

Significant effort has been made in the last decade to develop the next generation contrast microbubbles with applications extending beyond the scope of diagnostic imaging. Bubble effects beyond simple backscattering—stable and inertial cavitation [18–20], microstreaming [19], radiation force generation [21–23], ultrasound-mediated destruction [24,25]—are being investigated for therapeutic applications like modulation of vascular and cellular permeability [26,27], thrombolysis [28,29] and gene delivery [30]. Novel ligand-mediated targeted imaging or molecular imaging are being developed that would allow noninvasive detection of physiological changes in patients at molecular and cellular levels [31–34]. Like liposomes, microbubbles can also be used as drug delivery vehicles for both hydrophobic [10] and hydrophilic [11,12] molecules, and achieve localized or targeted delivery through ultrasound-mediated destruction and/or other external triggers. Such drug release strategies can be used for treatment of cancer and atherosclerotic plaques [35]. A number of reviews have been published in this field [7,28,31,35–40]. Figure 1a shows a schematic representation of an ultrasound contrast microbubble with drug delivering capabilities. Instead of lipids, other materials can be used in the stabilizing encapsulation as mentioned earlier. Hydrophilic drugs can be loaded on the surface, whereas water insoluble drugs can be loaded within the oil layer in between the encapsulation and perfluorocarbon core. Electrostatic and ligand mediated interactions can also be utilized to load drugs outside the microbubbles. Figure 1b shows the various drug loading strategies utilized for contrast microbubbles.

In spite of the rapid development of microbubble based ultrasound contrast agents, clinical applications are often limited due to potential safety concerns [18,42,43] and lower circulation time [35]. The relatively larger size of microbubbles in comparison to nanometer sized pores observed in the leaky vasculature associated with cancerous tissues [35] and the constraints on the drug payload [44] also reduces their applicability in cancer therapy as drug delivery agents. These limitations motivated researchers to explore the possibility of ELIP that combine the favorable properties of microbubble based contrast agents and the drug delivering liposomes. Since their discovery in 1965, by Bangham [45,46], liposomes have been used extensively as drug delivery vehicles. Liposomes are typically nanometer sized vesicles with a hydrated lipid bilayer encapsulating an aqueous phase. The bilayer membrane is spontaneously formed due to thermodynamic interactions when phospholipids are dispersed in an

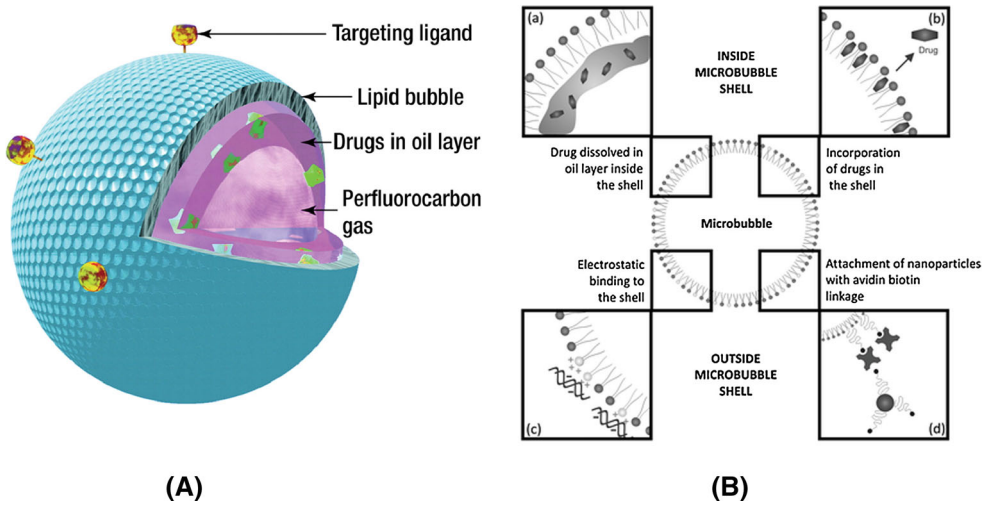

Fig. 1 **a** Schematic representation of a contrast microbubble constructed for drug-delivery (Reproduced with permission from [41]) **b** Drug loading strategies implemented with contrast microbubbles (Reproduced with permission from [40])

aqueous phase [47]. Structurally, liposomes are very similar to biological cells. Hence, liposomes offer several favorable properties like longer circulation time in the blood stream, lesser toxicity, and increased uptake by target organs/tissues, making them suitable for use as drug delivery vehicles [48–51]. Currently, there are about 10 liposomal drug formulations approved by the FDA for human use [48,52]. Liposomes conjugated with targeted ligands can achieve active targeting of intended sites [51]. Several exogenous (e.g., temperature [53], light [54]) and endogenous (e.g., pH [55], enzymes [56,57], redox [58]) triggers have been used to make stimuli-responsive drug delivery vehicles. Such formulations offer local control over payload release resulting in reduced systemic toxicity. Recently, ultrasound has also been investigated as possible external trigger for releasing liposomal contents [48,49,59,60].

Acoustically responsive liposomes were first reported in 1996 [61] and termed ELIPs. The preparation protocol was later optimized by Huang and co-workers [62–64] through years of research to establish a standardized methodology involving 3–5 freeze-thaw cycles and lyophilization in presence of a weak cryoprotectant mannitol. These steps are critical in ensuring the echogenicity (i.e. capability to scatter incident acoustic waves effectively) of these liposomes. It is hypothesized that the freeze-thaw and lyophilization in presence of mannitol creates bilayer defects, which later allow the entrapment of air during reconstitution [65,66]. Presence of entrapped air makes these liposomes echogenic. Although, echogenicity of these liposomes have been conclusively demonstrated through both in vitro [66,67] and in vivo [68] experiments, the exact location of entrapped air remains uncertain. Possible explanations are the existence of a gas pocket within the bilayer [52,63,69] or presence of a lipid monolayer coated bubble floating within the aqueous compartment [63]. Since, ELIPs retain all the favorable properties of normal liposomes [52], they have also been investigated for simultaneous imaging and ultrasound mediated drug release studies [69–76]. Figure 2 below shows two hypothetical structures of ELIP. ELIPs can be loaded with both hydrophilic and lipophilic drugs represented in the figure by fluorescent green circles and red boxes respectively. Like microbubbles, liposomes can also be prepared with ligand mediated targeting properties. Another strategy to incorporate favorable properties of microbubbles and liposomes in the same formulation can be conjugation of gas filled microbubbles and liposomes. Several groups have also been investigating such microbubble-liposome conjugates [77–79].

In light of the above discussion, it can be concluded that microbubbles and liposomes hold great potential for clinical imaging and therapeutic applications. Their realization will depend on understanding of the physical principles behind their behaviors through experiments and mathematical modeling. Following sections will a give an overview of such studies undertaken in our laboratory along with some specific examples that can motivate future research.

3 Bubble dynamics

3.1 Free bubble dynamics

Gas bubbles are an intriguing physical system primarily due to their complex non-linear dynamics. The dynamics of uncoated gas bubbles have been studied extensively both mathematically and experimentally [80,81]. The bubble dynamics is governed by the Rayleigh–Plesset (RP) equation [82–86]:

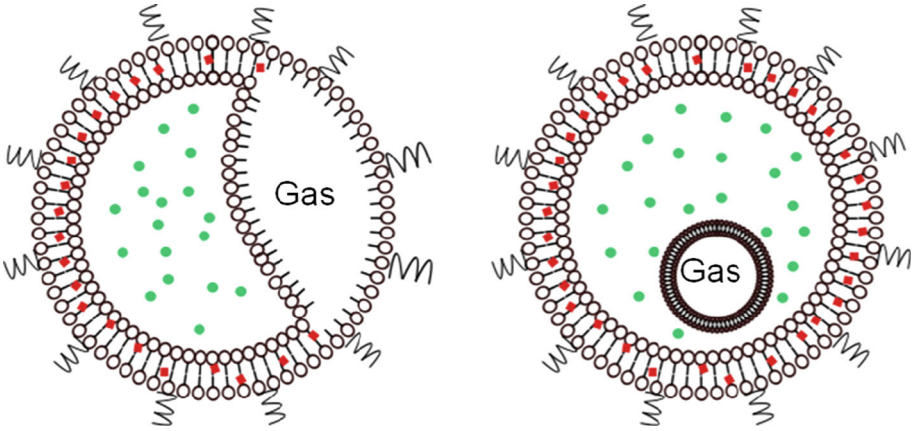

Fig. 2 Hypothesized structure of echogenic liposomes (ELIPs)

$$\rho\left(R\ddot{R}+\frac{3}{2}\dot{R}^2\right)=P_G-\frac{2\gamma}{R}-4\mu\frac{\dot{R}}{R}-P_0+p_A(t), \tag{1}$$

where R is the instantaneous radius of the spherical bubble, $\dot{R}$ and $\ddot{R}$ are the first and second order time derivatives of the bubble radius, ρ is the density of the surrounding liquid, P_G is the pressure of the gas inside the bubble, μ is the liquid viscosity, γ is the gas-liquid surface tension, P_0 is the ambient pressure, and $p_A(t)$ is the time dependent excitation pressure. Note that the classical RP equation (1) assumes the surrounding liquid to be incompressible. Several modifications of the RP equation, e.g., Keller–Miksis equation [87], Trilling Equation [88], Herring equation [89], and Gilmore equation [90] have been suggested to include liquid compressibility. Prosperetti and Lezzi [91–93] in their pioneering work proved that these equations are essentially members of the same family of differential equations, but it remains difficult to ascertain which equation will give the most accurate numerical results. Brenner and co-workers [94], suggested that the following form of the RP equation, which also incorporates liquid compressibility, is stable at high Mach numbers.

$$\rho\left(R\ddot{R}+\frac{3}{2}\dot{R}^2\right)=P_G-\frac{2\gamma}{R}-4\mu\frac{\dot{R}}{R}-P_0+p_A(t)-\frac{R}{c}\frac{dP_G}{dt}, \tag{2}$$

where the last term (c is the speed of sound) is the correction due to compressibility. If the gas inside is assumed to obey a polytropic law and diffusion is neglected, the inside gas pressure can is given by

$$P_G=P_{G0}\left(\frac{R_0}{R}\right)^{3k}, \tag{3}$$

where R_0 the initial bubble radius, P_{G0} is the initial gas pressure and k is the polytropic exponent. Incorporating (3) in (2), we obtain the following form of compressible RP equation:

$$\rho\left(R\ddot{R}+\frac{3}{2}\dot{R}^2\right)=P_{G0}\left(\frac{R_0}{R}\right)^{3k}\left(1-\frac{3k\dot{R}}{c}\right)-\frac{2\gamma}{R}-4\mu\frac{\dot{R}}{R}-p_0+p_A(t). \tag{4}$$

3.2 Encapsulated bubble dynamics

3.2.1 A brief review of the existing models for encapsulated microbubbles

Two recent articles [95,96] present excellent reviews of the topic. The earliest attempt to model dynamics of contrast microbubbles dates back to 1990, where Roy and co-workers [97] modeled the encapsulation as a viscous liquid. de Jong and others modeled Albunex [98–101], the first clinically approved contrast agent, by including ad hoc terms—shell friction and elasticity factors—in the RP equation which nonetheless represented the correct physics that the encapsulation is a viscoelastic shell. The first rigorous theoretical model was developed by Church [102], where he assumed the encapsulation material to be an incompressible solid with a linear viscoelastic constitutive equation, which effectively represented a Kelvin–Voigt type relation. Hoff et al. [103] modified this model by incorporating a thin shell approximation, and matched the model predictions with the experimental data for Nycomed. Morgan et al. [104] proposed a modified Herring equation with an elastic term derived using Glazman's approach [105], to describe the encapsulated bubble dynamics. Khismatullin and Nadim [106] introduced compressibility and viscoelasticity in the surrounding liquid, and showed that that they have negligible effects on the dynamics. Allen et al. [107] assumed the encapsulation to be a purely viscous liquid layer, with bulk viscosity parameters to model the encapsulation of an experimental therapeutic microbubble named MRX-552 (ImaRx Therapeutics, Tucson, AZ, USA). Allen and Rashid [108] later proposed another model to predict large amplitude oscilla-

tions of polymeric spheres that can be used to model polymer coated microbubbles.

In 2003, our group proposed, for the first time, an interfacial rheological model for contrast agent encapsulation [109]. We argued that the encapsulation which is typically a few molecule thick—most often a monolayer—cannot be assumed to be a homogeneous continuum with bulk material properties (viscosity and elasticity) at least in the thickness direction. Clearly, the three orders of magnitude separation of length scale between the overall dimension of the microbubble (micrometer) and the thickness of the encapsulation (nanometer) warrants a proper multi-scale approach; treating them simultaneously would be a prohibitively costly computational task. Therefore interfacial rheology, where the interface is treated as a zero-thickness surface with complex interfacial properties—as opposed to bulk rheological properties—that effectively represent the thickness averaged material response, is the appropriate approach for modeling the encapsulation. Note that the surface tension used to characterize an air–liquid interface, either pure or contaminated with surfactants, is also an interfacial rheological property [109]. Over the years, we have developed a two-pronged interfacial rheological characterization effort which includes one experiment to determine the characteristic properties of the encapsulation and a second independent experiment that validates the characterization [109–112]. The independent validation distinguishes this effort from other similar modeling studies. It also incorporates a way to improve a model where sophistication is introduced as warranted by the modeling effort as opposed to prescribed in advance. In 2003, we adopted the simplest interfacial rheology—Newtonian, i.e., purely viscous with a constant surface tension (γ_0) and a dilatational viscosity (κ^s). We determined these two parameters for a number of contrast agents using attenuation of ultrasound through a contrast agent suspension. However, we obtained an unreasonably large value of surface tension (∼0.7–40 N/m) compared to the value (0.072 N/m) of a pure air–water interface [109], whereas one would expect a lower value due to the absorption of the surface-active molecules at the interface. Accordingly in 2005, we developed a new model—constant elasticity model—including an interfacial dilatational elasticity (E^s) [110]. Characterization with this model obtained a more reasonable surface tension value (smaller than the pure air water interface). However, the model performed poorly in validation, i.e., the predicted scattered subharmonic response did not match well with experimental measurement [110]. We attributed the failure to the shortcoming of the linearity—constant dilatational elasticity—for predicting nonlinear scattering. In 2010, we implemented an exponential strain-softening dilatational elasticity to account for the large amplitude non-linear oscillations in 2010 [111]. The model performed very well in predicting the behaviors of contrast agent Sonazoid [111].

Meanwhile, Marmorttant et al. [113] introduced a linear viscoelastic model with a radius dependent surface tension. The model is equivalent to our constant elasticity model—the parameter χ here being the same as E^s—except that it accounts for rupture and buckling of the encapsulation. The Marmottant model has gained wide acceptability because of its ability to predict several non-linear behaviors of lipid shells—e.g. compression only behavior, where the bubbles compresses more than they expand. Doinikov and Dayton [114] in 2007, proposed a model for lipid shelled microbubbles assuming the shell to be a viscoelastic Maxwell fluid. Tsiglifis et al. [115] implemented three different constitutive laws, viz., Kelvin-Voigt, Mooney-Rivlin, and Skalak models to describe the elastic properties of the encapsulating shell. Stride [116] in 2008, proposed a model for contrast agent encapsulation by treating it as a homogenous insoluble molecular monolayer with both viscosity and interfacial tension varying with the instantaneous molecular concentration at the interface. Doinikov et al. [117] proposed another model with a non-linear viscosity term in addition to the Kelvin-Voigt elasticity term to better predict non-linear behavior of lipid shells. Marmottant et al. [118] have also proposed a recent modification of their existing model for lipid encapsulation to extend its applicability to solid like encapsulating shells. In an attempt to explain the variation of estimated properties with bubble size, Li et al. [119] have proposed an integration of the nonlinear elasticity of the Marmottant model with the nonlinear viscosity proposed by Doinikov and coworkers to have a 'nonlinear shell elasticity and viscosity' model (NSEV).

3.2.2 *Mathematical formulation of encapsulated bubble dynamics*

The different models to describe dynamics of encapsulated microbubbles discussed in the preceding paragraph are essentially modified versions of the classical Rayleigh–Plesset equation that can be represented in a single framework [120]:

$$\rho\left(R\ddot{R}+\frac{3}{2}\dot{R}^2\right)=P_{G_0}\left(\frac{R_0}{R}\right)^{3k}\left(1-\frac{3k\dot{R}}{c}\right)-\frac{2}{R}\gamma\,(R) -\frac{4\dot{R}}{R^2}\kappa^s(R,\dot{R})-4\mu\frac{\dot{R}}{R}-p_0+p_A(t), \tag{5}$$

where $\gamma\,(R)$ is the effective surface tension and $\kappa^s(R)$ is the effective dilatational viscosity. One can linearize Eq. (5) and express it in the form of linear harmonic oscillator:

$$\ddot{x}+\omega_0\delta\dot{x}+\omega_0^2x=F(t). \tag{6}$$

The linearized equation can be used to obtain the damping coefficient (δ) and the resonance frequency ($\omega_0 = 2\pi f_0$).

The damping term has three separate contributions one each from liquid viscosity, shell viscosity and acoustic radiation:

$$\delta = \frac{1}{\rho\omega_0 R_0^2}\left(\underbrace{4\mu}_{\text{Viscous}} + \underbrace{4\frac{\kappa^s}{R_0}}_{\text{Encapsulation}} + \underbrace{\frac{3kP_{G0}R_0}{c}}_{\text{Radiation}}\right). \tag{7}$$

The total damping and the resonance frequency are useful for estimating model material parameters of the encapsulation. The contribution due to the thermal damping requires more rigorous treatment [121–123], and hence difficult to include in a simplified form. Moreover, most of the available thermal damping models are developed for linear oscillations with limited validity in the non-linear regime. Hence, thermal damping is either neglected—assuming nearly isothermal or adiabatic oscillations—or included through an additional thermal viscosity term just like the viscous damping due the surrounding liquid. Usually thermal damping is negligible in comparison to the encapsulation damping for contrast agents [124,125], but one must be aware that such assumptions might not always be valid. The mathematical descriptions of the interfacial rheological models proposed by our group are discussed in the next section.

3.2.3 *Interfacial rheological models for UCA encapsulations*

(A) Newtonian model (NM) [109,110]

As mentioned above, here the encapsulation of a contrast microbubble was modeled as a purely viscous interface of infinitesimal thickness:

$$\gamma(R) = \gamma(\text{constant}),\ \kappa^s(R) = \kappa^s(\text{constant}). \tag{8}$$

The resonance frequency is given by

$$f_0 = \frac{1}{2\pi R_0}\sqrt{\frac{1}{\rho}\left(3kp_0 + \frac{2\gamma}{R_0}(3k-1)\right)}. \tag{9}$$

We estimated the properties of an encapsulation by fitting a model prediction to experimentally measured attenuation data. As noted before, for several commercial contrast agents like Sonazoid and Optison this model predicted unrealistically large values for surface tension ($\sim$ 0.6–40 N/m) [109,110] due to the absence of an interfacial elasticity term in the model.

(B) Constant elasticity viscoelastic Model (CEM) [110]

This model assumes a constant dilatational elasticity and viscosity:

$$E^s = \left(\frac{\partial\gamma}{\partial\beta}\right)_{\beta=0},$$
$$\gamma(R) = \begin{cases} \gamma_0 + E^s\beta & \text{for } \gamma_0 + E^s\beta > 0 \\ 0 & \text{for } \gamma_0 + E^s\beta \le 0 \end{cases} \quad \text{and}$$
$$\kappa^s(R) = \kappa^s(\text{constant}), \tag{10}$$

where $\beta = \left(\frac{\Delta\text{Area}}{\text{Area}_{\text{equilibrium}}}\right) = \left(\frac{R^2}{R_E^2} - 1\right)$ is the fractional change in area from an unstrained or stress free position (radius R_E) and γ_0 is the reference surface tension at that radius. The equilibrium radius (R_E) is given by $R_E = R_0\left(1 - \frac{\gamma_0}{E^s}\right)^{-\frac{1}{2}}$. This ensures a balance of inside and outside pressure at initial radius. The resonance frequency is given by

$$f_0 = \frac{1}{2\pi R_0}\sqrt{\frac{1}{\rho}\left(3kp_0 - \frac{4\gamma_0}{R_0} + \frac{4E^s}{R_0}\right)}. \tag{11}$$

Using CEM led to a reasonable value for surface tension lower than the air-water interface.

(C) Viscoelastic model with exponentially varying elasticity (EEM) [111]

The inability of the CEM model to match the experimentally observed subharmonic thresholds as per experimental observations led us to propose nonlinear strain-softening [111]. We proposed two simple non-linear extensions of the constant elasticity (Hooke's law)—elasticity varying linearly with area fraction i.e. a quadratic elasticity model (QEM), and an exponentially varying elasticity model (EEM). They both performed equally well in predicting the subharmonic response. Since the exponential variation of surface elasticity seems more physical we implemented it for all our subsequent numerical investigations of contrast agent dynamics. The effective surface tension term and viscosity terms of the EEM is given below

$$\gamma(R) = \begin{cases} \gamma_0 + E^s\beta & \text{for } \gamma_0 + E^s\beta > 0 \\ 0 & \text{for } \gamma_0 + E^s\beta \le 0 \end{cases} \quad \text{and}$$
$$\kappa^s(R) = \kappa^s(\text{constant}), \tag{12}$$

where $E^s = E_0^s\beta\exp(-\alpha^s\beta)$, $\beta = \left(\frac{R^2}{R_E^2} - 1\right)$. Enforcing the balance of pressure at initial radius, we have an expression of equilibrium radius given by $R_E = R_0\left[1 + \left(\frac{1-\sqrt{1+4\gamma_0\alpha^s/E_0^s}}{2\alpha}\right)\right]^{-1/2}$. The resonance frequency due to EEM is given as

$$f_0 = \frac{1}{2\pi R_0}\sqrt{\frac{1}{\rho}\left(3kp_0 + \frac{2E_0^s}{R_0}\left(\frac{\sqrt{1+4\gamma_0\alpha^s/E_0^s}}{\alpha^s}\right)\left(1+2\alpha^s-\sqrt{1+4\gamma_0\alpha^s/E_0^s}\right)\right)}. \tag{13}$$

Note that in general one can have $\gamma(R)$ negative, i.e. the encapsulation is in compressive stress. However, one can also impose that under compression the encapsulation buckles and effectively the surface tension becomes zero [15]. Imposition of such non-negativity leads to compression-only behavior but usually predicts higher subharmonic thresholds [111]. The results shown here are obtained using the constant elasticity and the exponential models without the condition of non-negativity imposed on them.

(D) Marmottant model (MM) [113,118]

The Marmottant model assumes the surface tension to have three distinct regimes: a buckled state of the encapsulation with zero surface tension below a prescribed buckling radius, an elastic state with linearly varying elasticity similar to the CEM, and a ruptured state with surface tension same as that of the air–water interface above a rupture radius. The effective surface tension and the viscosity terms due to this model are given as

$$\gamma(R) = \begin{cases} 0 & \text{for} \quad R \le R_{\text{buckling}} \\ \chi\left(\frac{R^2}{R_{\text{buckling}}^2}-1\right) & \text{for} \quad R_{\text{buckling}} \le R \le R_{\text{break-up}} \\ \gamma_w & \text{if ruptured and for } R \ge R_{\text{rupture}} \end{cases} \quad \text{and } \kappa^s(R) = \kappa^s(\text{constant}), \tag{14}$$

where χ [identical to E^s in (9)] is the elastic modulus of the shell, $R_{\text{buckling}} = R_0\left[1+\frac{\gamma(R_0)}{\chi}\right]^{-1/2}$, and $R_{\text{rupture}} = R_0\left[1+\frac{\gamma_{\text{water}}}{\chi}\right]^{-1/2}$ Although such an effective surface tension behavior is physically quite realistic, the choice for the different limiting radii remains hard to determine, and typically made so that the results match with experimental observations. The breakup radius is difficult to estimate and is usually considered to be same as the rupture radius. We also assumed $\gamma(R_0)$ to be zero for all the simulations presented in this paper. It ensures a pressure equilibrium at the initial unstrained state. Note that due to the discontinuous variation of effective surface tension with radius, it is difficult to give an expression of the resonance frequency. However, one can derive the expression assuming that the bubble exists completely in the elastic regime:

$$f_0 = \frac{1}{2\pi R_0}\sqrt{\frac{1}{\rho}\left(3kp_0 - \frac{2\gamma(R_0)}{R_0}(3k-1) + \frac{4\chi}{R_0}\right)}. \tag{15}$$

Recently smoother forms of Marmottant model have been proposed that involves a smoothing near the discontinuities [126,127]. One such form is given below

$$\begin{aligned}\gamma(X) &= \chi[H(X-X_{\text{buckling}}) - H(X-X_{\text{rupture}})] \\ &\quad + \gamma_0 H(X-X_{\text{rupture}}), \\ X &= R_0(1+X) \text{ and } \gamma_0 = \gamma(R_0)\end{aligned} \tag{16}$$

where H is the Heaviside step function which can be smoothed by a Peskin cosine function to avoid sharp transitions as shown below

$$H_\varepsilon(x) = \frac{1}{2} + \frac{(\varepsilon/\pi)\sin\pi x/\varepsilon}{2\varepsilon}. \tag{17}$$

3.2.4 *Estimation of model parameters describing encapsulation rheology*

Estimation of model parameters remains a difficult problem to date. Standard low frequency techniques for direct measurement of interfacial properties such as Langmuir trough are of limited validity for measuring material properties of contrast agents oscillating at megahertz frequencies. Hence, several different approaches have been utilized to measure material properties using various experiments, e.g., backscattering measurements [128], attenuation measurements[66, 109–111,129,130], light scattering experiments [131,132], high-speed optical observations [124,133–135], atomic force microscopy [136] and measurements using fluorescence recovery after photobleaching (FRAP) [137], fluorescence lifetime imaging [138].

We use the experimentally obtained attenuation data to determine the unknown model parameters and then validate our model predictions against nonlinear scattering [110–112]. Usually, attenuation experiments are performed at low amplitude excitations. Hence, one can use the linearized version of RP equation to get expressions for both the damping coefficient [See (7)] and the resonance frequency [See (9), (10), (12), (14)]. A least square minimization is used with the error function:

$$Er(\gamma, \kappa^s, \cdots) = \sum_i \left[\alpha(\omega_i) - \alpha^{meas}(\omega_i)\right]^2, \tag{18}$$

where $\alpha^{meas}(\omega)$ is the experimentally measured attenuation coefficient and $\alpha(\omega)$ is the theoretical prediction of attenuation coefficient which can be calculated using the following expression

$$\alpha(\omega) = 10\log_{10} e \int_{R_{\min}}^{R_{\max}} \sigma_e(R;\omega) n(R) dR,$$
$$\text{where } \sigma_e = 4\pi R_0^2 \frac{c\delta}{\omega_0 R_0} \frac{\Omega^2}{[(1-\Omega^2)^2 + \Omega^2\delta^2]} \text{ and } \Omega = \frac{\omega_0}{\omega}, \tag{19}$$

where e is the base of the natural logarithm, $n(R)dR$ is the number of bubble per unit volume within the radius range $(R, R+dR)$, and total range of bubble radii in the distribution is given by $(R_{\max}, R_{\min})$. A Matlab® (Mathworks, Natick, MA, USA) code is used to obtain the model parameters using the above technique. Hughes et al. [139] and Grishenkov et al. [140] suggested a more stringent test by simultaneously fitting both attenuation and phase velocity for PVA-shelled microbubbles. Due to the ill posed nature of the problem, the fitting process is difficult and also very sensitive to several factors like polydispersity of the suspension, initial guess of parameters, etc. [112]. Also, attenuation data might not always reflect the linearized dynamics. Recent experimental observations have demonstrated the occurrence of non-linear behaviors e.g., compression only behavior [141], shift of resonance frequency [141], subharmonic generation [126], etc., even at very low acoustic excitation pressures of 50 kPa. This may result in inaccurate predictions.

3.2.5 Prediction of encapsulated bubble dynamics and scattering

Once the interfacial rheological properties of the encapsulation corresponding to a specific model have been determined, one can solve Eq. (5) using standard numerical techniques for solving stiff ordinary differential equations. We use the ode15s solver in Matlab® with the initial conditions of $R(t=0) = R_0$ and $\dot{R}(t=0) = 0$. The scattered pressure $P_s(r,t)$and scattering cross-section $\sigma_s(r,t)$ are also calculated from the radial dynamics [142]:

$$P_S(r,t) = \rho\frac{R}{r}\left(2\dot{R}^2 + R\ddot{R}\right) \text{ and}$$
$$\sigma_s(r,t) = \frac{4\pi\left\langle r^2 P_s(r,t)^2\right\rangle}{P_A^2}. \tag{20}$$

We obtain the scattered response spectrum using the fast Fourier transform (FFT) and integrating the contributions from all the bubbles of different radii ranging from $R_{\min}$ to $R_{\max}$ using

$$S_s(\omega) = \int_{R_{\min}}^{R_{\max}} \sigma_s(R;\omega) n(R) dR. \tag{21}$$

The peak values corresponding to different frequencies of interest can be extracted from the FFT, and utilized for model validation purposes as shown in subsequent sections. Note that (20) assumes absence of multiple scattering effects. If undetermined model parameters are estimated by use of experimentally measured radial dynamics, the numerical solution of the RP equation can be directly fitted with data.

4 Characterization of ultrasound contrast microbubbles

This section sketches acoustic characterization techniques for ultrasound contrast microbubbles. Although encapsulated microbubbles are also being developed as targeted drug delivery vehicles with stimuli responsive release properties, a discussion of those studies are omitted here for brevity. Along with the review of existing literature, specific results for both attenuation and scattering data will also be presented as illustrative examples for two different contrast microbubbles viz., Sonazoid TM(GE Healthcare, Oslo, Norway)[1] with a phospholipid coating and poly(DL-lactic acid) polymer (PLA) encapsulated microbubbles. The preparation protocol of Sonazoid, a commercially available contrast agent, is unavailable. The PLA microbubbles were developed by Prof. Margaret A. Wheatley at the Biomedical Engineering Department, Drexel University [11,12,143–148]. The detailed description of the experimental setups used to study acoustic scattering from and attenuation through a suspension of above mentioned contrast agents can be found in our earlier publications [110,112,149], and hence, not discussed here.

4.1 Attenuation and estimation of interfacial rheological properties

Attenuation measures the loss of energy of an acoustic wave as it travels through a medium. It is enhanced in presence of microbubbles. If the attenuation due to the contrast microbubbles is too high, the scattered signal can be lost completely before being received by the transducers. Hence, the earliest standardized measurements of contrast agent efficacy utilized a parameter called scattering to attenuation cross-section ratio (STAR). For a good contrast agent this value should be as high as possible indicating a high backscatter of signal with minimal loss of energy of the scattered wave during transmission. Apart from a measure of contrast

[1] Development suspended in USA and EU. It is currently approved for use in Japan.

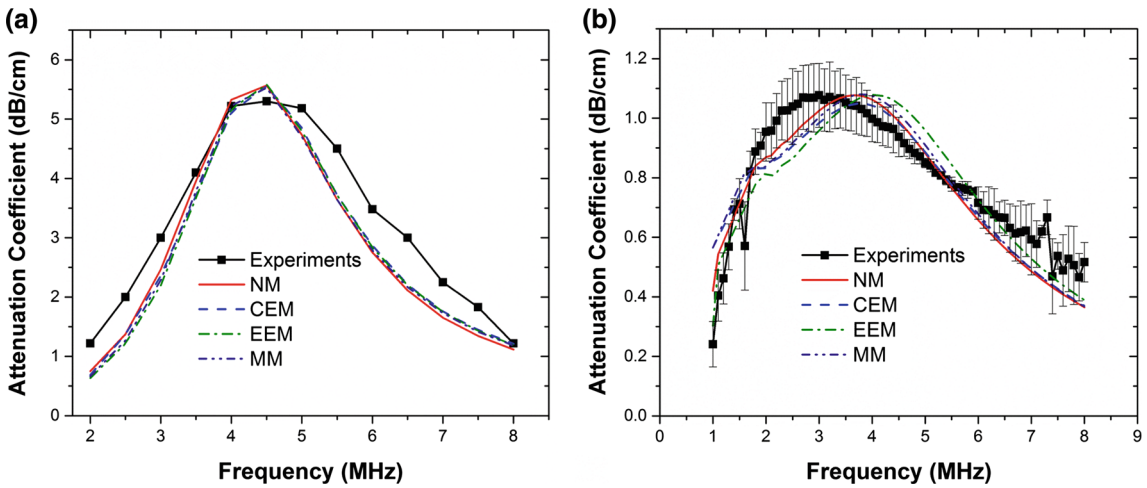

Fig. 3 Experimentally measured and fitted attenuation data for **a** Sonazoid (Reproduced with permission from [110] and [111]). **b** PLA microbubbles (Reproduced with permission from [112]). *NM* Newtonian model, *CEM* constant elasticity model, *EEM* exponential elasticity model, *MM* Marmottant model

agent efficacy, the frequency dependent attenuation measurement can also capture the resonance behavior of a monodisperse bubble population as evident from (18). The peak in attenuation curve indicates the resonance frequency. For a polydisperse suspension the peak will indicate a weighted average resonance frequency. Note that multiple scattering effects can be neglected for attenuation experiments due to low concentration of microbubbles [129]. A linear increase of attenuation with microbubble concentration indicates the validity of this assumption. If the attenuation measurements are acquired at low enough excitation pressure, the dynamics can be described by the linearized bubble dynamics equation.

Figure 3a shows the frequency dependent attenuation data acquired experimentally for Sonazoid microbubbles at a concentration of 8.1×10^4 bubbles/ml solution. It also shows the best fitting obtained with different models for encapsulations using the technique mentioned in Sect. 3.2.4. Fitting was executed with an average size (1.6 μm) and the total number concentration. Figure 3b shows similar experimental data for PLA microbubbles at a concentration of 4.0×10^4 bubbles/ml of solution and the best fitting curves for various models with the full size distribution; using an average size with PLA resulted in unsatisfactory results owing to the effects of polydispersity as mentioned earlier in Sect. 3.2.4.

For estimation of properties, we used $\rho = 1,000$ kg/m ^{3}, $\mu = 0.001$ kg/ m s , $c = 1485$ m/s , $p_0 = 101325$Pa. The values of polytropic constant (k) used were 1.07 for Sonazoid bubbles and 1.00 for air-filled PLA bubbles. Note that the choice of polytropic exponent is a non-trivial problem. Using an analysis due to Prosperetti [121], which is valid for small amplitude oscillations, we determined the oscillations are nearly adiabatic for Sonazoid bubbles (perfluorocarbon gas inside) and nearly isothermal for PLA microbubbles (air filled). However, such simplifications might not be valid for large amplitude non-linear oscillations, and a more rigorous approach might be required [150,151]. Table 1 provides the estimated material properties of the encapsulation for both Sonazoid and PLA microbubbles. Note the difference in estimated properties for the two different kinds of encapsulation. The Newtonian model predicts surface tension value for Sonazoid (~ 0.6 N/m) that are higher than the air–water interfacial tension value 0.072 N/m and physically unrealistic. The predictions improve with incorporation of elasticity in the rheological model. For PLA microbubbles however the Newtonian model predicts low surface tension values. Hence, the introduction of elasticity results in prediction of elasticity values (~ 0.05 N/m) that are an order of magnitude smaller than those predicted for the lipid encapsulation. In fact, for this very reason, for PLA bubbles, even the Newtonian model fares very well.

4.2 Nonlinear scattering experiments and model validation

The predictive capabilities of different models are judged by their ability to capture experimentally observed dynamics. We argue that the model validation should be done against experiments other than the one used for model parameter estimation. We have followed such an approach in our lab—the model parameters are determined using attenuation and then the full nonlinear RP equation with the estimated property values is numerically solved to calculate the far field scattered pressure. The model predictions are compared against experimental data for both fundamental and subharmonic scattered responses. Since the fundamental response can be matched very accurately even with the linearized version of RP equations [111], the performance of the models is judged by its ability to predict the scattered nonlinear response.

Table 1 Estimated interfacial rheological properties of the encapsulation of Sonzaoid and PLA microbubble for different interfacial models

Interfacial model	Sonazoid TM	PLA microbubbles
Newtonian model (NM)	$\gamma = 0.60 \pm 0.14$ N/m $\kappa^s = 1.0 \pm 0.004 \times 10^{-8}$ N·s/m	$\gamma = 0.06 \pm 0.03$ N/m $\kappa^s = 6.0 \pm 3.5 \times 10^{-9}$ N·s/m
Constant elasticity model (CEM)	$\gamma_0 = 0.02$ N/m $E^s = 0.51 \pm 0.11$ N/m $\kappa^s = 1.0 \pm 0.004 \times 10^{-8}$ N·s/m	$\gamma_0 = 0.01 \pm 0.006$ N/m $E^s = 0.05 \pm 0.03$ N/m $\kappa^s = 6.0 \pm 3.5 \times 10^{-9}$ N · s/m
Exponential elasticity model (EEM)	$\gamma_0 = 0.02$ N/m $E^s = 0.55 \pm 0.10$ N/m $\kappa^s = 1.2 \pm 0.40 \times 10^{-8}$ N · s/m $\alpha = 1.5$	$\gamma_0 = 0.01 \pm 0.006$ N/m $E_0^s = 0.05 \pm 0.03$ N/m $\kappa^s = 6.0 \pm 3.5 \times 10^{-9}$ N · s/m $\alpha = 1.5$
Marmottant model (MM)	$\gamma_0 = 0.0$ N/m (i.e. $R_{\text{buckling}} = R_0$) $\chi = 0.53 \pm 0.10$ N/m $\kappa^s = 1.2 \pm 0.40 \times 10^{-8}$ N · s/m $R_{\text{break-up}} = 1.5 R_{\text{buckling}}$	$\gamma_0 = 0.0$ N/m (i.e. $R_{\text{buckling}} = R_0$) $\chi = 0.06 \pm 0.02$ N/m $\kappa^s = 6.0 \pm 3.5 \times 10^{-8}$ N · s/m $R_{\text{break-up}} = 1.5 R_{\text{buckling}}$

Most of the imaging applications utilize the fundamental response—the response obtained at the frequency of excitation—from contrast microbubbles. However, due to the interference with signals originating from surrounding tissues, they often result in a poor signal to noise ratio (SNR). Due to their nonlinear nature, only contrast microbubbles can generate subharmonic response—response at half the excitation frequency—which can provide better SNR [152,153]. Hence, subharmonic imaging has been widely studied [154–158]. Subharmonic imaging has also been investigated for high frequency imaging applications [159–162] and noninvasive blood pressure estimation [163–174]. We have been investigating scattered subharmonic response from contrast microbubbles both experimentally and through numerical simulations [110–112,120,125,175]. Figure 4 below shows both the experimentally measured and simulated subharmonic responses from Sonazoid and PLA coated microbubbles. Note that the excitation pressure dependent subharmonic curves show all the typical features where there is no subharmonic response below a threshold pressure followed by a rapid rise beyond threshold and eventual saturation of the response. The simulated responses from various models are obtained by solving the full RP type equation with estimated properties given in Table 1.

As seen in the Fig. 4, the generation of subharmonic occurs only when a certain threshold excitation is exceeded. Our previous studies [111,120,125] have shown that interfacial models with nonlinear elasticity term viz., EEM and MM, can predict subharmonic thresholds accurately. Nonlinear interfacial rheology was found to be required to describe the large amplitude oscillations of contrast microbubbles.

4.3 Radial dynamics of contrast microbubbles

Measuring material properties using attenuation through a bulk suspension of microbubbles have several limitations e.g., polydispersity of microbubbles affects the predictions, linearized dynamics might not be a valid assumption, the material properties might not be the same over the entire range of bubble population etc. Due to these limitations associated with attenuation, experimentally obtained radius-time signatures of microbubble are also used for the estimation of interfacial properties. The radial dynamics of individual microbubble can be captured directly using high speed cameras [135,176,177] and streak cameras [104,178–180] or indirectly e.g., using light scattering measurements [131,132,181] and an acoustical camera [182]. Although, direct optical observations of microbubbles offer several advantages like more accurate measurement, isolation of response from individual microbubble, minimal effects of signal attenuation and no requirement of accurate calibration, they often have limited optical resolution, constraints over data collection, and require ultra-fast cameras that are expensive and not easily accessible. Indirect measurements provide an inexpensive, less complicated, real-time alternative with no limitations on the data acquisition. However, they cannot provide the wide-range visual information obtained from direct optical observations. Techniques using radius-time data have been successful in accurately capturing the radial dynamics of several different contrast microbubbles like Quantison® [183], Definity® [132,184], SonoVue [131,135,176,185], BR14 [124,126,182] Sonazoid [181], Optison® [181], Targestar [186] etc. The numerical solution of the RP type equation can be fitted with these experimentally measured radius-time curves to obtain the material properties using an error minimization algorithm mentioned earlier. The fitting can be done with just the knowledge of the bubble's initial radius and the excitation pulse. It has been successfully implemented to estimate model parameters for different encapsulated microbubbles using several different rheological models of encapsulation [117,119,124,131,132,176]. Several interesting observations have been made during experimental investigations of the radial dynamics of contrast microbubbles like compression-only behavior [113,141,185], existence of a threshold for the onset of oscillations [141,187], mode vibration of bubbles

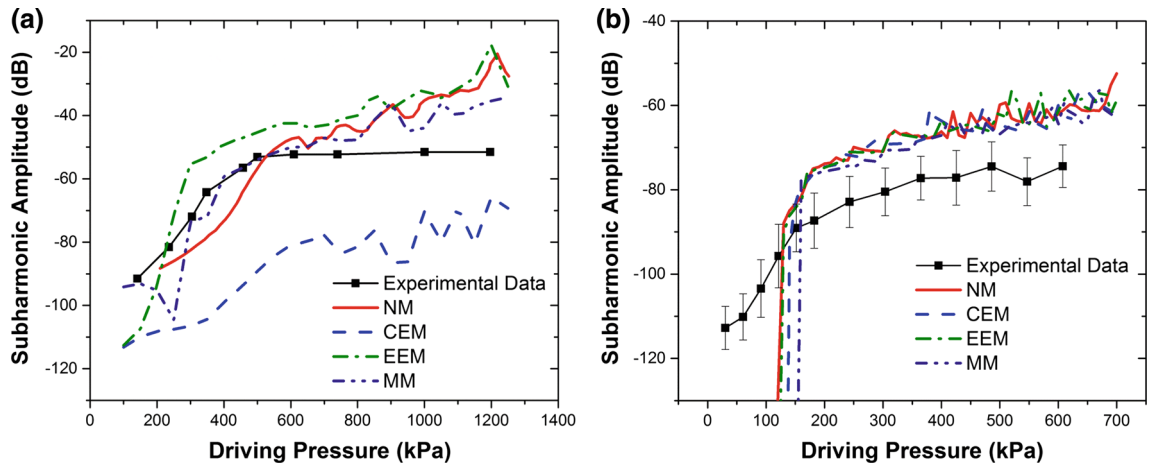

Fig. 4 Comparison of experimentally measured and predicted scattered sub-harmonic responses based on the different interfacial models for **a** Sonazoid microbubbles at 2 MHz excitation (Reproduced with permission from [110] and [111]). **b** PLA microbubbles at 2.25 MHz excitation (Reproduced with permission from [112])

[188,189], non-spherical oscillations [189–191], buckling of shells [192] etc. These observations reflect the nonlinearity of the encapsulated bubble dynamics even at low acoustic excitation pressures, which is neglected in fitting the linearized dynamics with experimental attenuation data. This gives a definite advantage to this kind of property estimation technique to assess the applicability and validity of various models. To illustrate this we can consider the compression-only behavior—at low excitation pressures, certain phospholipid coated bubbles (e.g., BR14, SonoVue) show asymmetric oscillations, more compression than expansion, about the initial diameter. This behavior has been attributed to the buckling of the phospholipid shells [192]. Most models for encapsulated bubble dynamics cannot capture this behavior except Marmottant's model [113], Doinikov's nonlinear viscosity model [117], the NSEV model [119] and the exponential elasticity model with non-negative surface tension. Thus, comparison with experimentally observed radius-time curves can also assess the capabilities of various rheological models and can be used for characterization of contrast agents.

As noted before, polydispersity poses a significant challenge for characterization and modeling. As a result, significant efforts have been made to develop single bubble acoustic characterization techniques [193–205]. An alternate approach has been to produce monodisperse bubble suspensions [206–210] and characterize them with standard attenuation and scattering experiments [206,208,211,212]. These efforts are critical for better understanding and improvement of rheological models of microbubble encapsulations.

5 Characterization of echogenic liposomes (ELIP)

Since the first report of ELIP, many studies have been undertaken for characterization of their behaviors. As noted before, they combine drug bearing capacity of liposomes with ability to respond to ultrasound stimulation. Here we will briefly discuss their preparation, acoustic characterization and drug release studies.

5.1 Preparation protocol of echogenic liposomes

The modified preparation protocol for preparing ELIP is critical for ensuring their acoustically responsive nature. The updated and detailed methodology proposed by Huang and co-workers [64] can be found in a recent publication. ELIPs can be prepared in a pressurized or a non-pressurized environment. The lipids are mixed in the desired molar ratio in a round bottomed flask and dissolved in an organic solvent e.g., choloroform. The solvent is then evaporated at 40 °C, usually in a rotary evaporator, to obtain a thin film. Residual traces of the solvent are removed by placing the flask under high vacuum overnight. The lipid films are then hydrated with a 0.32 M mannitol solution in buffer. The hydrating solution can also contain hydrophilic molecules, which will be encapsulated within the aqueous core of the liposomes. The mutilamellar vesicles, formed after the hydration, are bath sonicated for 10 min. The resulting solution of liposomes is frozen at −70 °C for 30 min followed by thawing at room temperature. Around 3–5 freeze-thaw cycles have been suggested for ELIP production [64]. The liposomes are again frozen at −70 °C and lyophilized in a freeze-drying apparatus. The lyophilized dry cake thus obtained is stored at 4 °C until further use. For the pressurization technique, the sonicated liposomal solution is collected in a screw-cap vial and pressurized by a gas using a syringe. The pressurized-gas/liposome dispersion is incubated for 30 min and then frozen at −78 °C on dry ice for another 30 min followed by immediate depressurization. The frozen liposomes are

thawed at room temperature to change the temperature from −78 to 24 °C within 10 min.

The lyophilized cakes of ELIPs, obtained either way, are reconstituted in a phosphate buffered saline (PBS) solution for further investigations. Adding 5 % by weight of bovine serum albumin (BSA) to the PBS prevents the aggregation of ELIPs [66] and substantially improves the detection of their acoustical reflectivity. The critical steps in the above-mentioned methodology for echogenicity of liposomes are freeze-thaw cycles and lyophilization in presence of mannitol, a weak cryoprotectant, and the subsequent reconstitution process. It has been proposed that the lipid bilayer develops defects during the freezing steps due to the weak cryoprotection abilities of mannitol [64], thereby exposing the hydrophobic portions of the lipid bilayer. The fluffy dry cake formed after lyophilization also increases the surface area of contact. The air is entrapped through these bilayer defects during the reconstitution phase form gas pockets stabilized by lipid monolayer [65,66]. The exact location or dimensions of this structure remains unascertained. Moreover, the protocol also does not guarantee that all the liposomes in the suspension will be associated with such a structure [64]. Nevertheless, the echogenicity of the liposomes prepared following this protocol has been conclusively demonstrated through several independent experiments including ones in our laboratory described below. Note that the preparation protocol can be further modified to include different lipid formulations and targeting ligands or to replace the entrapped air with other bioactive gases. Two such novel ELIP formulations with simultaneous imaging and targeted delivering capabilities have been developed by us and will be discussed in a later section.

5.2 Acoustic characterization of echogenic liposomes

Earliest studies of the echogenicity of ELIPs primarily employed a 20 MHz high frequency intravascular ultrasound (IVUS) catheter for both in vitro [61,62] and in vivo [65,68,69,213] characterization. Subsequently their design was optimized using the same probe as well as videodensitometric analysis [63,214].

The first comprehensive in vitro characterization of ELIP was performed by Coussios et al. [215]. They used a 3.5 MHz lightly focused immersion transducer and compared the echogenicity of ELIPs with that of the microbubble based contrast agent Optison®. They reported that the backscattering coefficient of liposomes can be even higher than that of Optison® with the liposomes having higher scattering-to-attenuation ratio (STAR). This demonstrated the potential of ELIPs to be used as ultrasound contrast agents.

Kopechek et al. [66] extended this study to a wider range of frequencies for both attenuation and backscattering experiments using single element immersion transducers. Unlike contrast microbubbles (Fig. 1), ELIPs showed no definite peak in broadband attenuation in the range of 3–25 MHz. The attenuation was fitted with the Church's model for encapsulated bubbles to predict a shear viscosity of 0.30 Pa·s and a shear modulus of 125 MPa. These values are equivalent to a dilatational viscosity $\kappa^s = 9 \times 10^{-10}$ N.s/m and a dilatational elasticity $E^s = 0.56$ N/m 0.56 N/m . They also reported a backscattering coefficient of 0.011–0.023 $(\text{cm-str})^{-1}$in the range of 6–30 MHz resulting in a STAR of 8–22 %, which is comparable with the values for contrast microbubbles.

We have also measured broadband attenuation and pressure dependent scattered response from ELIPs using single element immersion transducers [67]. We found no peak in attenuation for a frequency range of 1–13 MHz. Scattering measurements, conducted at 3.5 MHz and 50–800 kPa, showed a 15–20 dB enhancement over control (i.e., in absence of ELIPs in suspension) at a lipid concentration of 1.67 μg/ml. Although the scattered response showed second-harmonic response, no subharmonic response was observed under these excitation conditions.

Lu et al. [216] followed a similar method to prepare ELIP with an average size of 1600 ± 200 nm and conducted in vitro acoustic studies. They also found no distinct peak in attenuation, but concluded that the resonance lies in the range 7–11 MHz. Their scattering experiments at 10 MHz excitation showed enhancement of both fundamental and second-harmonic responses. These liposomes were not found to be very robust with an effective operation time of 10 min and a destruction threshold of 150 kPa at 2.25 MHz excitation. Authors also detected echogenicity of such liposomes with 25 MHz B-mode pulses. Using a Phillips L12-5 linear array transducer system [217], ELIPs were found to generate robust echoes for both continuous 6–9 MHz fundamental and 4–5 MHz harmonic B-mode pulses. A more recent in vitro study by Radhakrishnan and co-workers [218] evaluated the performance of ELIPs as a blood pool contrast agent using a physiologic flow phantom. ELIPs were found to be stable in physiologic conditions with proper care. Around 14–17 dB enhancement of echogenicity was reported in citrate–phosphate–dextrose whole blood. Echogenicity was reported to be sensitive to abnormalities of red blood cells and rapid cooling below body temperature. Suitability of ELIPs as contrast agents for passive cavitation imaging have also been reported [219].

We have recently reported echogenicity of several modified ELIP formulations [75,76] thereby demonstrating their potential for development as therapeutic ultrasound contrast agents. The ELIP formulations were tested for echogenicity using an in vitro acoustic setup employing single element focused ultrasound transducers. Unlike our other studies, here all the acoustic characterizations were done at 3.5 MHz frequency and at an acoustic excitation pressure of 500 kPa

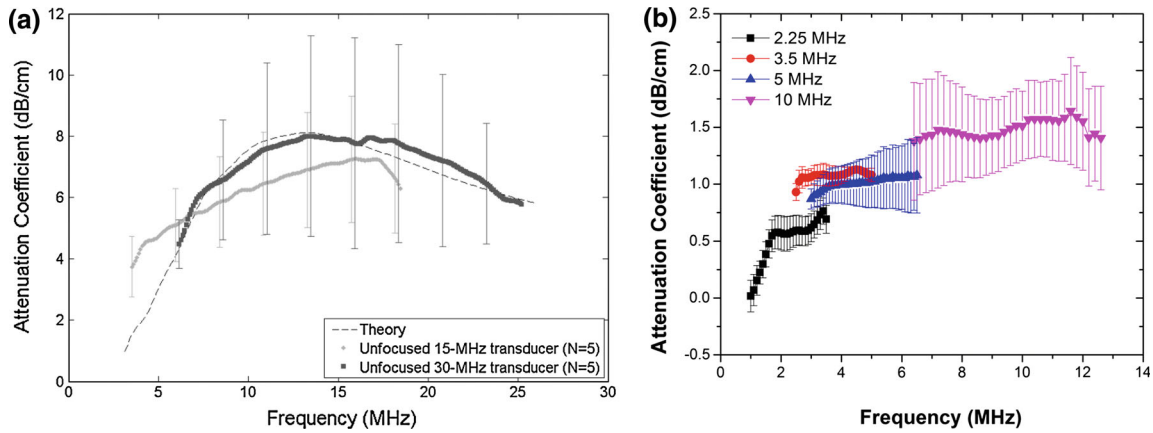

Fig. 5 Frequency dependent broadband attenuation measurements form ELIP suspensions reported by [64] Kopechek et al. (Reproduced with permission from [66]) at a lipid concentration of 0.05 mg/ml and **b** Paul et al. (Reproduced with permission from [67]) at a lipid concentration of 10μg/ml ELIP

with a 32 cycle sinusoidal pulse. The ELIPs were also imaged using a diagnostic ultrasound scanner (Terason t3200, MedCorp LLC., Tampa, FL, USA). Sax and Kodama [220] have also prepared ELIPs encapsulating perfluoropropane gas to study their stability in vitro and in vivo by varying their lipid compositions. Echogenicity measurements were acquired using a high frequency US imaging system generating B-mode pulses. They reported that increasing the molar ratio of polyethylene glycol (PEG) lipids significantly enhanced the half-life of the liposomes, both in vitro (55 MHz probe) and in vivo (40 MHz probe). However, in contrast to previous reports, cholesterol was shown to reduce stability of the liposomes by increasing membrane permeability and gas leakage.

Figure 5 shows a comparison of the attenuation measurements by Kopechek et al. with that conducted in our laboratory. The flat nature of the attenuation curves in both set of experiments can be attributed to the highly polydisperse size distribution of ELIPs that can range from nanometer sized to micron sized particles. The larger error bars associated with the attenuation data from both the previous reports can be attributed to the inherent variability in the acoustic properties of ELIPs, possibly again due to their high polydispersity. It should also be mentioned that Kopechek et al. assumed the volume of the gas pocket to be 18 % of the entire range of liposomal size to obtain the fitting. Since, no conclusive experiments have validated this assumption, we did not attempt to fit our attenuation data with any model to obtain material parameters. Moreover, most conventional sizing techniques like dynamic light scattering and Coulter counter measurements might not be accurate for such highly polydisperse size distribution. In fact, in spite of following the same protocol, the size distributions reported by Kopechek et al. and our measurements were significantly different (Table 2). Detailed studies on exact location of the gas pockets and their dimensions along with more reliable size distribution data will be essential for better understanding the underlying mechanisms of ELIP behavior. Nevertheless, thorough in vitro acoustic studies conclusively demonstrated the echogenic nature of this new variation of liposomes which was an essential step in the validation of the proof of concept.

Table 2 Comparison of previously reported size distribution measurements with ELIPs

	Kopechek et al.	Paul et al.
Size corresponding to the largest number density	65 nm	∼ 150 nm
Range of particle size detected [a]	30 nm–6 μm	100 nm–2μm
Polydispersity index (PDI)	Not reported	0.63–1.00

[a] Kopechek et al. concatenated size distributions from DLS (0–450 nm) and Coulter Counter (450 nm or above)

As mentioned earlier, freeze drying in presence of mannitol is critical for ELIP [62,63,65]. Although there are conflicting reports of optimal mannitol concentration during preparation [62,69], the established protocol suggests the use of 320 mM considering both echogenicity and encapsulation efficiency of the liposomes [63]. We have investigated in detail the effects of mannitol concentration on echogenicity [67]; a finite amount of mannitol was found to be essential for acoustic reflectivity of the ELIPs. We also found that liposomes were only echogenic when they were lyophilized in presence of mannitol for different ELIP formulations.

As mentioned above, although these studies have demonstrated the potential of ELIPs as ultrasound contrast agents, there remains important unanswered questions relating to the exact cause of echogenicity. There is a need to determine the exact location and dimension of gas pockets. This problem has eluded researchers since the first report of ELIP, fueling the skepticism regarding their echogenicity. There have been microscopic pictures that suggests gas pockets [66,67,76,221]. However, the pictures are not as conclusive

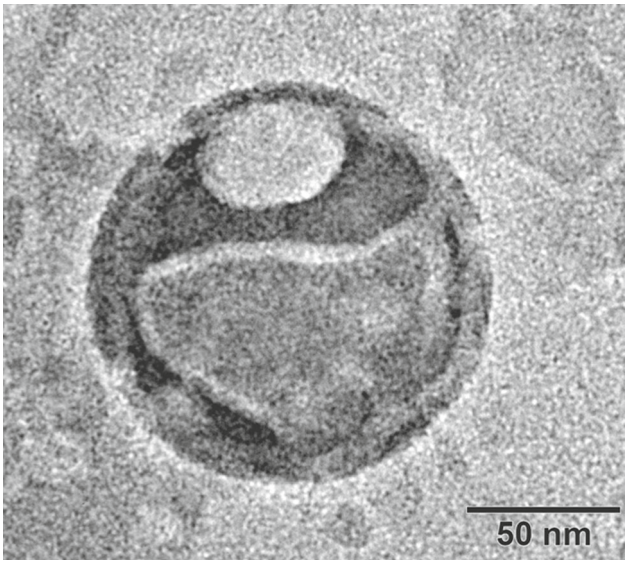

Fig. 6 Transmission electron micrographic image of a negatively stained polymer coated ELIP with 1 % phosphotungstic acid, captured using a JEOL JEM-2100-LaB_6 microscope at 200 kV (Reproduced with permission from [76])

as one would like them to be so that it can end the decade long debate about these purported gas pockets. In our personal experience, these pictures have been extremely difficult to obtain. Figure 6 shows a transmission electron microscopic (TEM) image of a polymer coated ELIP obtained by our group. A gas pocket similar to that shown in the hypothesized structure presented in Fig. 2 can be seen. Even if these gas pockets exist, their dimensions will be too small to have a scattering cross-section large enough to be detected accurately by 1–10 MHz acoustic waves. On the other hand, experimental evidence clearly shows that the echogenicity is only achieved when the modified preparation protocol is followed. We believe that the echogenicity is primarily due to the existence of a smaller fraction of larger liposomes, which will have larger gas pockets. Presence of larger vesicles is indicated by the high polydispersity index of dynamic light scattering measurements with ELIP suspensions. Atomic force microscopic images (AFM), shown in Fig. 7, also show the presence of different sized vesicles, even with micron range diameters. However, due to the lack of conclusive evidence, existence of separate lipid monolayer coated microbubbles in the suspension, which may be created during the preparation of liposomes, cannot be completely ruled out.

5.3 Stimuli responsive release characteristics of echogenic liposomes

Since ELIPs retain all the favorable properties of normal liposomes, they have been extensively studied as ultrasound triggered drug delivery vehicles [52,74,222,223]. Anti-intercellular adhesion molecule-1 (ICAM-1) [224–227], anti-vascular cell adhesion molecule (VCAM-1), anti-fibrin, anti-fibrinogen and anti-tissue factor conjugated with ELIPs [68,228] have also been developed to achieve both in vitro and in vivo targeting. ELIPs can be loaded with both hydrophilic and lipophilic molecules [70]. By suitably modifying the preparation protocol, ELIPs have been made to entrap genes [229], fluorescent molecules like calcein [63,69,70,76] and carboxyfluorescein [75] as drug surrogates, antibiotics [230], peroxisomal proliferator-activated receptor agonists [231], a thrombolytic enzyme rt-PA (recombinant tissue-plasminogen activator) [74,223,232–234], a vasodilator papverine [70,235], an anti-diabetic drug rosiglitazone [236,237] and NF-κB decoy oligonucleotides [222]. By virtue of its preparation protocol, ELIPs can encapsulate a gaseous phase, which is usually air. However, with suitable manipulations of the preparation protocol, ELIPs can also encapsulate bioactive gases like xenon [238] and nitric oxide [239–241]. Note that in all these studies, incorporation of a payload did reduce the echogenicity of ELIPs significantly.

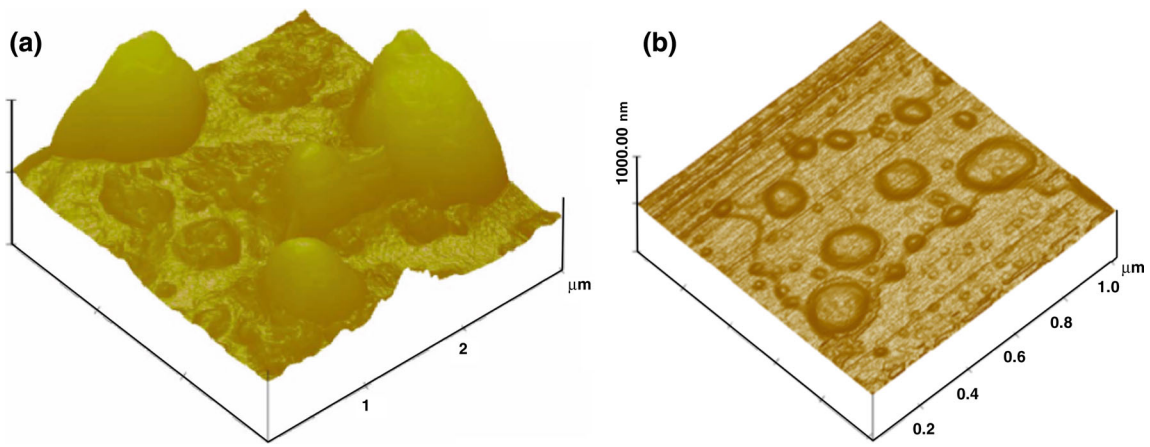

Fig. 7 Multimode^{TM} atomic force microscopic images of **a** Conventional ELIPs (reproduced with permission from [67]), and **b** Polymer coated ELIPs (reproduced with permission from [76])

Fluorescent molecules like calcein [77,242,243] and carboxyfluorescein [244,245] are often used as surrogates for hydrophilic drugs for evaluating triggered release from liposomes. Hence, ultrasound triggered release from ELIPs has also been studied by detecting changes in fluorescence due to the release of calcein or carboxyfluorescein. Huang and McDonald [69] used a continuous wave ultrasound pulse at 1 MHz frequency and at an output power of 2 W/cm ^{2}, generated using a Sonitron ultrasound system, for a duration of 10 s. Depending on the number of excitation cycles, 30–60 % release of contents was reported with no mention of passive release in absence of ultrasound. Huang et al. [63] in a later study used a similar ultrasound system to excite calcein loaded ELIPs with 1 MHz continuous wave ultrasound at 8 W/cm ^{2} output power for a duration of 10s. The passive and ultrasound triggered release (over 10 s) from air containing ELIPs was both around 10 % indicating negligible effects from ultrasound excitation. The release improved to about 30 % with argon or perfluorocarbon encapsulated ELIPs. Note that none of these studies reported the calibration techniques for determining the actual output power. Kopechek et al. [246] did a detailed calibration of Sonitron systems to show that presence of standing waves can play a critical role in the above mentioned in vitro studies-the pressure field can be corrupted due to the constructive and destructive interference. A more detailed study of ultrasound mediated release of calcein was performed by Kopechek and co-workers [70] using color Doppler ultrasound. A CL15-7 linear array transducer was used to generate 6 MHz ultrasound pulses at 2 MPa peak-negative pressure and a PRF of 150 Hz. Although 47.5 $\pm$ 33 % release of calcein was reported with ultrasound, no release was observed for the lipophilic drug papaverine in the same study. However, a later study by the same group concluded that the results might be erroneous due to effects of gas bubbles on fluorescence measurements [237]. The same study, which used 6 MHz color Doppler ultrasound pulses (1,250 Hz PRF and 0.17 W/cm^2 calibrated output power) from CL15-7 transducer, reported no ultrasound mediated release of calcein and rosiglitazone, even after detection of both inertial and stable cavitation. Smith et al. [74] have also shown therapeutically relevant release of rt-PA from ELIPs using color Doppler ultrasound. Other studies have demonstrated thrombolytic efficacy of rt-PA loaded ELIPs [223,232,247] Buchanan et al. [222] had studied ultrasound mediated release of oligonucleotides (ODN) using a Sonitron 1000 system to generate 1 MHz continuous wave ultrasound at a peak negative pressure of 0.26 MPa for a duration of 60s. Around 42 % release of ODN from ELIPs was reported compared to around 18 % release from non-echogenic liposomes. However, it is not clear if their measurements are also susceptible to changes caused by the presence of gas bubble as mentioned earlier.

Table 3 Ultrasound parameters used in the release studies with two different ELIP formulations with dual triggers

Type of echogenic liposome	Ultrasound parameters
MMP-9 cleavable ELIPs	Frequency: 3 MHz
	Duty cycle: 100 %
	Peak negative output pressure: 3 MPa
	Duration of exposure: 3 min
Redox triggered ELIPs	Frequency: 3 MHz
	Duty cycle: 100 %
	Peak negative output pressure: 0.53 MPa
	Duration of exposure: 2 min

It is evident from the preceding discussions that ultrasound mediated release of liposomal contents is often uncertain and susceptible to several other factors that can critically affect the release efficiency. Moreover, the release is not always optimal, ranging from 20 to 50 %. This motivated us to pursue the development of ELIP with dual release triggers-a combination of a different exogenous or endogenous trigger with ultrasound-to achieve considerable higher amount of contents release. To date we have developed two such ELIP formulations: a substrate lipopeptide conjugated ELIP formulation that can be triggered (or cleaved) by the extracellular enzyme matrix metalloproteinase-9 (MMP-9) [75] and a polymer coated redox triggered ELIP formulation capable of cytosolic drug delivery [76]. MMP-9 is overexpressed in atherosclerotic diseases and in metastatic cancers [248–253]. We have also developed an ELIP formulation with pH tunable echogenicity [unpublished work].

For our drug release studies, we used a single element flat faced ultrasound transducer that has been carefully calibrated to determine accurately the output energy of the ultrasound pulse. The transducer was excited with a 3 MHz continuous wave ultrasound pulse. The output pressure and duration of excitation was chosen for optimal release of contents under static conditions (Table 3). For a set of positive control experiments, we also utilized a 22.5 kHz sonic dismembrator at 4 W output setting.

For the MMP-9 cleavable ELIPs, carboxyfluorescein was encapsulated to quantify the release of liposomal contents by employing a self-quenching strategy. Figure 8a shows ultrasound enhanced recombinant MMP-9 triggered release of contents from the ELIPs. About 50–60 % release was observed with recombinant MMP-9 enzymes whereas a 30–50 % release was observed with conditioned cell culture media from cancer cells secreting MMP-9. This release was further enhanced by 10–15 and 20–30 % for recombinant enzyme and conditioned media respectively by the application of ultrasound. Note that negligible release (4 %) was seen when only ultrasound was used to trigger release. Also,

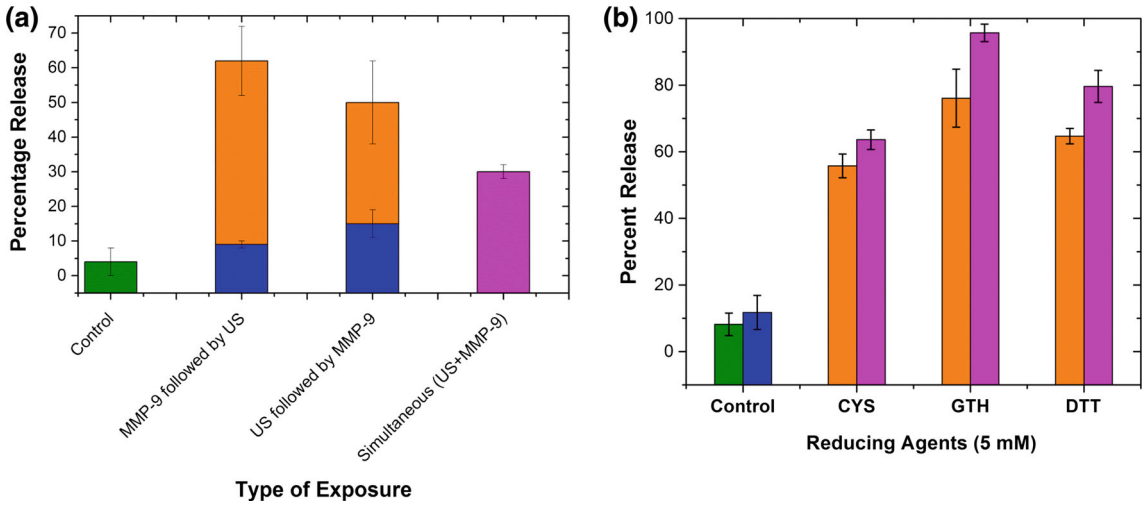

Fig. 8 **a** Ultrasound (US) enhanced recombinant MMP-9 triggered release of contents from MMP-9 cleavable ELIPs. **b** Ultrasound (US) enhanced redox triggered release of contents from polymer coated disulfide cross-linked ELIPs (Reproduced with permission from [76]). In both the figures, the olive, blue, orange, and magenta colored bars represents the passive release in absence of any trigger, release due to US only, release due to other triggers (MMP-9 or redox) only, and the release with simultaneous application of US and the other trigger respectively

the simultaneous application of ultrasound and enzymatic trigger showed a reduction in release, possibly due to localized increase of temperature during ultrasonic excitation that reduced the activity of the recombinant enzymes (bulk temperature was maintained constant by using an ice bath). It should also be mentioned that we utilized the non-lyophilized version of the liposomes for our release studies. Hence, we do not expect any interference in our fluorescence measurements due to presence of gas bubbles.

The polymer coated ELIPs had a disulfide cross-linkage that is stable in mildly oxidizing environment but unstable in presence of reducing agents. Typically cytosolic concentration of reducing agents is higher than that in plasma and extracellular matrix [254]. Hence, this disulfide crosslinker has been effective for cytosolic drug delivery [255–257] using the reversible disulfide thiol conversion [254]. In order to achieve active internalization of the ELIPs in cancer cells, we incorporated a folate conjugated lipid in the ELIPs. A $CoCl_2$ quenching strategy was implemented to quantify release of calcein from these polymer coated ELIPs in the presence of both redox and ultrasound triggers. Negligible release (less than 5 %) was observed in our control samples i.e., both without ultrasound and reducing agents. At a very low concentration of glutathione (5 μM, corresponds to its concentration in extracellular matrix), the release was also less than 5 %, but it increased significantly with increasing reducing agent concentration. We were able to obtain up to 90 % release with just reducing agents at 10 mM concentrations (typical in cell cytoplasm). As with the MMP-9 cleavable ELIPs, there was no release with just the application of 3 MHz ultrasound. However, about 8–20 % enhancement over redox triggered release was observed with simultaneous application of 5 mM redox and ultrasound. Figure 8b shows the release of liposomal contents from these liposomes with dual triggers—ultrasound and reducing agents. Different reducing agents were used for comparison, which includes dithiothreitol (DTT), cysteine (CYS) and glutathione (GSH).

6 Summary and scope for future research

Encapsulated microbubbles and ELIPs are being rapidly developed for several of diagnostic imaging applications as well as targeted drug delivery for treatment of cardiovascular diseases and several types of cancer. This review, although provides more details on recent research performed by our group, was intended to provide a broad overview of the progress in this field of research and motivate future research. Several clinical and therapeutic applications of both encapsulated microbubble based ultrasound contrast agents and ELIPs were discussed to familiarize the reader with developments in this field over the past few decades.

We present a review of the various modeling strategies proposed till date for encapsulated microbubbles along with a detailed discussion of the newly proposed interfacial models. Several different experimental techniques for characterization of encapsulated microbubble dynamics are then discussed. Estimation of the rheological properties of the encapsulation by various models remains a difficult task. Various experimental strategies employed for this are also discussed briefly with a detailed overview of the hierarchical approach used in our lab. The predictive capabilities of the different interfacial models are discussed with specific examples of Sonzoid and poly(DL-lactic acid) polymer

(PLA) encapsulated microbubbles by comparing experimentally measured subharmonic responses with model predictions. The interfacial models with nonlinear elasticity and/or viscosity are found to be better equipped to capture complex encapsulated bubble dynamics. Some relevant analytical results for subharmonic thresholds are also presented for better understanding of model predictions.

We also present a comprehensive review of the characterization of the acoustic properties and stimuli responsive release properties of ELIPs. Echogenic liposomes are often found to behave differently from conventional microbubble based contrast agents. A critical analysis of the various hypotheses for their echogenicity is also presented to initiate further research interests.

As evident from the preceding discussion, the recent developments in interfacial models have significantly improved our understanding of encapsulated bubble dynamics, and equipped us with powerful predictive tools of contrast agent behavior. However, none of the models enjoys unambiguous validity and each comes with a set of strengths and weaknesses. Moreover, emerging experimental techniques are reporting several new and interesting contrast agent behaviors. Therefore, further experiment driven model improvement is required to improve their reliability and widen their scope of applicability. Clinical applications of contrast agents involve polydisperse bubble population at fairly high concentrations. Model predictions are critically dependent on the bubble size distributions. Therefore, more reliable and accurate size measurements techniques are required especially those which can handle highly polydisperse systems. Increasing levels of sophistications and complexity can be introduced into modeling e.g. multiple scattering [258], presence of blood vessels [259–261], non-spherical bubble oscillations [188,262], ultrasound mediated bubble destruction, and effects of drug loading and targeting ligands on bubble dynamics [263,264]. Experimental characterization of encapsulated bubble dynamics also have several potential areas for further development e.g., devising sophisticated experimental techniques for correct estimation of shell viscoelastic properties, accounting for polydispersity of bubble suspensions during experiments, characterization of nonlinear behavior at low acoustic pressure, characterization of bubble-wall interactions, determination of the thresholds for subharmonic generation, characterization of rupture, break-up, dissolution dynamics of encapsulated bubbles etc.

Acoustic measurements with ELIPs have conclusively demonstrated their potential for applications as ultrasound contrast agents. However, the exact mechanisms for their echogenicity are not completely understood primarily due to the uncertainty regarding the exact location of the gas pockets. As is obvious from the review above, due to such lack of understanding, unlike microbubble contrast agents, there has not been much progress in modeling behaviors of ELIPs. The only model [66], as mentioned above, estimated the gas volume to be certain percentage of the entire liposomal population, and computed attenuation. Only an accurate knowledge of the locations and dimensions of the gas pockets will enable us to develop improved mathematical models of their acoustic behaviors. The high polydispersity of ELIPs also pose an important hurdle for better mathematical characterization and hence, requires sophisticated size measurement techniques that can handle such wide range of particle sizes in the same suspension. Considering the experimental results for stimuli responsive release from ELIPs, it can be safely concluded that ELIPs can be potentially used for simultaneous imaging and therapeutic applications. If implemented successfully, such contrast agents can provide powerful treatment strategies for several cardiovascular diseases and cancer. However, there also is a need for detailed parametric study of ultrasound mediated release form ELIPs in vitro using clinically relevant ultrasound pulses to ascertain the optimal excitation conditions. It will be also be beneficial to detect the role of cavitation associated with such release. Such studies will improve our understanding of the physical mechanisms, and pave the way for clinical translation of these technologies.

Acknowledgments This research was supported by NIH Grants 1R01 CA 113746, 1R01 CA 132034, NSF Grant DMR 1005011 to SM and DMR-1005283, CBET 1033256, CBET 1205322 to KS.

References

1. Liu J et al (2006) Nanoparticles as image enhancing agents for ultrasonography. Phys Med Biol 51:2179–2189
2. Gao Z et al (2008) Drug-loaded nano/microbubbles for combining ultrasonography and targeted chemotherapy. Ultrasonics 48:260–270
3. Rhyner MN et al (2006) Quantum dots and multifunctional nanoparticles: new contrast agents for tumor imaging. Nanomedicine 1:209–217
4. Phillips D et al (1998) Acoustic backscatter properties of the particle/bubble ultrasound contrast agent. Ultrasonics 36:883–892
5. Waggoner AD et al (2001) Guidelines for the cardiac sonographer in the performance of contrast echocardiography: recommendations of the American Society of Echocardiography Council on Cardiac Sonography. J Am Soc Echocardiogr 14:417–420
6. Mulvagh SL et al (2000) Contrast echocardiography: current and future applications. J Am Soc Echocardiogr 13:331–342
7. Klibanov AL (2002) Ultrasound contrast agents: development of the field and current status. Contrast Agents Ii 222:73–106
8. Postema M, Gilja OH (2011) Contrast-enhanced and targeted ultrasound. World J Gastroenterol 17:28–41
9. Liu J-B et al (2005) Contrast-enhanced ultrasound imaging: state of the art. J Med Ultrasound 13:109–126
10. Phillips LC et al (2011) Localized ultrasound enhances delivery of rapamycin from microbubbles to prevent smooth muscle proliferation. J Controlled Release 154:42–49
11. Eisenbrey JR et al (2010) Development and optimization of a doxorubicin loaded poly(lactic acid) contrast agent for ultrasound directed drug delivery. J Controlled Release 143:38–44

12. Eisenbrey JR et al (2010) Delivery of encapsulated doxorubicin by ultrasound-mediated size reduction of drug-loaded polymer contrast agents. IEEE Trans Biomed Eng 57:24–28
13. Gramiak R, Shah PM (1968) Echocardiography of the aortic root. Investig Radiol 3:356–366
14. Hilgenfeldt S et al (1998) Response of bubbles to diagnostic ultrasound: a unifying theoretical approach. Eur Phys J B 4:247–255
15. Katiyar A et al (2009) Effects of encapsulation elasticity on the stability of an encapsulated microbubble. J Colloid Interface Sci 336:519–525
16. Sarkar K et al (2009) Growth and dissolution of an encapsulated contrast microbubble. Ultrasound Med Biol 35:1385–1396
17. Postema M, Schmitz G (2006) Bubble dynamics involved in ultrasonic imaging. Expert Rev Mol Diagn 6:493–502
18. Miller DL et al (2008) Bioeffects considerations for diagnostic ultrasound contrast agents. J Ultrasound Med 27:611–632
19. Wu J, Nyborg WL (2008) Ultrasound, cavitation bubbles and their interaction with cells. Adv Drug Deliv Rev 60:1103–1116
20. Coussios CC, Roy RA (2008) Applications of acoustics and cavitation to noninvasive therapy and drug delivery. Annu Rev Fluid Mech 40:395–420
21. Dayton P et al (1999) Acoustic radiation force in vivo: a mechanism to assist targeting of microbubbles. Ultrasound Med Biol 25:1195–1201
22. Dayton PA et al (2002) The magnitude of radiation force on ultrasound contrast agents. J Acoust Soc Am 112:2183–2192
23. Dayton PA et al (1997) A preliminary evaluation of the effects of primary and secondary radiation forces on acoustic contrast agents. IEEE Trans Ultrason Ferroelectr Freq Control 44:1264–1277
24. Casciaro S et al (2007) Experimental investigations of nonlinearities and destruction mechanisms of an experimental phospholipid-based ultrasound contrast agent. Investig Radiol 42:95–104
25. Chatterjee D et al (2005) Ultrasound-mediated destruction of contrast microbubbles used for medical imaging and drug delivery. Phys Fluids 17:100603
26. Ward M et al (1999) Ultrasound-induced cell lysis and sonoporation enhanced by contrast agents. J Acoust Soc Am 105:2951–2957
27. Ward M et al (2000) Experimental study of the effects of optison (R) concentration on sonoporation in vitro. Ultrasound Med Biol 26:1169–1175
28. Unger EC et al (2004) Therapeutic applications of lipid-coated microbubbles. Adv Drug Deliv Rev 56:1291–1314
29. Xie F et al (2005) Effectiveness of lipid microbubbles and ultrasound in declotting thrombosis. Ultrasound Med Biol 31:979–985
30. Taniyama Y et al (2002) Local delivery of plasmid DNA into rat carotid artery using ultrasound. Circulation 105:1233–1239
31. Bull JL (2007) The application of microbubbles for targeted drug delivery. Expert Opin Drug Deliv 4:475–493
32. Christiansen JP, Lindner JR (2005) Molecular and cellular imaging with targeted contrast ultrasound. Proc IEEE 93:809–818
33. Klibanov AL (2006) Microbubble contrast agents—targeted ultrasound imaging and ultrasound-assisted drug-delivery applications. Investig Radiol 41:354–362
34. Lindner JR (2004) Molecular imaging with contrast ultrasound and targeted microbubbles. J Nucl Cardiol 11:215–221
35. Ferrara K et al (2007) Ultrasound microbubble contrast agents: fundamentals and application to gene and drug delivery. Annu Rev Biomed Eng 9:415–447
36. Bekeredjian R et al (2005) Use of ultrasound contrast agents for gene or drug delivery in cardiovascular medicine. J Am Coll Cardiol 45:329–335
37. Hernot S, Klibanov AL (2008) Microbubbles in ultrasound-triggered drug and gene delivery. Adv Drug Deliv Rev 60:1153–1166
38. Lindner JR (2004) Microbubbles in medical imaging: current applications and future directions. Nat Rev Drug Discov 3:527–532
39. Martin KH, Dayton PA (2013) Current status and prospects for microbubbles in ultrasound theranostics. Wiley interdisciplinary reviews. Nanomed Nanobiotechnol 5(4):329–345
40. Lentacker I et al (2009) Drug loaded microbubble design for ultrasound triggered delivery. Soft Matter 5:2161–2170
41. Blomley MJK et al (2001) Microbubble contrast agents: a new era in ultrasound. BMJ 322:1222–1225
42. Main ML et al (2009) Ultrasound contrast agents: balancing safety versus efficacy. Expert Opin Drug Saf 8:49–56
43. Haar G (2009) Safety and bio-effects of ultrasound contrast agents. Med Biol Eng Comput 47:893–900
44. Klibanov AL et al (2010) Ultrasound-triggered release of materials entrapped in microbubble-liposome constructs: a tool for targeted drug delivery. J Controlled Release 148:13–17
45. Bangham A (1989) The 1st description of liposomes—a citation classic commentary on diffusion of univalent ions across the lamellae of swollen phospholipids by Bangham AD, Standish MM, and Watkins JC. Curr Contents Life Sci: 14–14
46. Bangham AD et al (1965) Diffusion of univalent Ions across lamellae of swollen phospholipids. J Mol Biol 13:238–252
47. Lasic DD (1998) Novel applications of liposomes. Trends Biotechnol 16:307–321
48. Lian T, Ho RJY (2001) Trends and developments in liposome drug delivery systems. J Pharm Sci 90:667–680
49. Torchilin VP (2005) Recent advances with liposomes as pharmaceutical carriers. Nat Rev Drug Discov 4:145–160
50. Moghimi SM, Szebeni J (2003) Stealth liposomes and long circulating nanoparticles: critical issues in pharmacokinetics, opsonization and protein-binding properties. Prog Lipid Res 42:463–478
51. Ding N et al (2011) Folate receptor-targeted fluorescent paramagnetic bimodal liposomes for tumor imaging. Int J Nanomed 6:2513–2520
52. Huang SL (2008) Liposomes in ultrasonic drug and gene delivery. Adv Drug Deliv Rev 60:1167–1176
53. Turner DC et al (2012) Near-infrared image-guided delivery and controlled release using optimized thermosensitive liposomes. Pharm Res 29:2092–2103
54. Leung SJ et al (2011) Wavelength-selective light-induced release from plasmon resonant liposomes. Adv Funct Mater 21:1113–1121
55. Hu FQ et al (2012) pH triggered doxorubicin delivery of PEGylated glycolipid conjugate micelles for tumor targeting therapy. Mol Pharm 9:2469–2478
56. Banerjee J et al (2009) Release of liposomal contents by cell-secreted matrix metalloproteinase-9. Bioconjug Chem 20:1332–1339
57. Sarkar N et al (2008) Matrix metalloproteinase-assisted triggered release of liposomal contents. Bioconj Chem 19:57–64
58. Ong W et al (2008) Redox-triggered contents release from liposomes. J Am Chem Soc 130:14739–44
59. Zhang L et al (2008) Nanoparticles in medicine: therapeutic applications and developments. Clin Pharmacol Ther 83:761–769
60. Schroeder A et al (2009) Ultrasound, liposomes, and drug delivery: principles for using ultrasound to control the release of drugs from liposomes. Chem Phys Lipids 162:1–16
61. AlkanOnyuksel H et al (1996) Development of inherently echogenic liposomes as an ultrasonic contrast agent. J Pharm Sci 85:486–490
62. Huang SL et al (2001) Improving ultrasound reflectivity and stability of echogenic liposomal dispersions for use as targeted ultrasound contrast agents. J Pharm Sci 90:1917–1926

63. Huang SL et al (2008) A method to co-encapsulate gas and drugs in liposomes for ultrasound-controlled drug delivery. Ultrasound Med Biol 34:1272–1280
64. Huang SL (2010) Ultrasound-responsive liposomes. In: Weissig V (ed) Liposomes, vol 605. Humana Press, New York, pp 113–128
65. Huang SL et al (2002) Physical correlates of the ultrasonic reflectivity of lipid dispersions suitable as diagnostic contrast agents. Ultrasound Med Biol 28:339–348
66. Kopechek JA et al (2011) Acoustic characterization of echogenic liposomes: frequency-dependent attenuation and backscatter. J Acoust Soc Am 130:3472–3481
67. Paul S et al (2012) In vitro measurement of attenuation and nonlinear scattering from echogenic liposomes. Ultrasonics 52:962–969
68. Hamilton AJ et al (2004) Intravascular ultrasound molecular Imaging of atheroma components in vivo. J Am Coll Cardiol 43:453–460
69. Huang SL, MacDonald RC (2004) Acoustically active liposomes for drug encapsulation and ultrasound-triggered release. Biochim Et Biophys Acta Biomembr 1665:134–141
70. Kopechek JA et al (2008) Ultrasound-mediated release of hydrophilic and lipophilic agents from echogenic liposomes. J Ultrasound Med 27:1597–1606
71. Huang SL et al (2002) Liposomes as ultrasound imaging contrast agents and as ultrasound-sensitive drug delivery agents. Cellul Mol Biol Lett 7:233–235
72. Tiukinhoy-Laing S et al (2005) Ultrasound-facilitated clot lysis using tPA-loaded echogenic liposomes. Circulation 112:U696–U696
73. Laing ST et al (2010) Ultrasound-mediated delivery of echogenic immunoliposomes to porcine vascular smooth muscle cells in vivo. J Liposome Res 20:160–167
74. Smith DAB et al (2010) Ultrasound-triggered release of recombinant tissue-type plasminogen activator from echogenic liposomes. Ultrasound Med Biol 36:145–157
75. Nahire R et al (2012) Ultrasound enhanced matrix metalloproteinase-9 triggered release of contents from echogenic liposomes. Mol Pharm 9:2554–2564
76. Nahire R et al (2013) Polymer-coated echogenic lipid nanoparticles with dual release triggers. Biomacromolecules 14:841–853
77. Klibanov AL et al (2010) Ultrasound-triggered release of materials entrapped in microbubble-liposome constructs: a tool for targeted drug delivery. J Controlled Release 148:13–17
78. Geers B et al (2011) Self-assembled liposome-loaded microbubbles: the missing link for safe and efficient ultrasound triggered drug-delivery. J Controlled Release 152:249–256
79. Kheirolomoom A et al (2007) Acoustically-active microbubbles conjugated to liposomes: characterization of a proposed drug delivery vehicle. J Controlled Release 118:275–284
80. Feng ZC, Leal LG (1997) Nonlinear bubble dynamics. Annu Rev Fluid Mech 29:201–243
81. Plesset MS, Prosperetti A (1977) Prosperetti, bubble dynamics and cavitation. Annu Rev Fluid Mech 9:145–185
82. Rayleigh L (1917) On the pressure development in a liquid during the collapse of a spherical cavity. Philos Mag 32(S8):94–98
83. Plesset M (1949) The dynamics of cavitation bubbles. ASME J Appl Mech 16:277–282
84. Noltingk BE (1950) Cavitation produced by ultrasonics. Proc Phys Soc Sect B 63:674–685
85. Neppiras EA (1951) Cavitation produced by ultrasonics: theoretical conditions for the onset of cavitation. Proc Phys Soc Sect B 64:1032–1038
86. Poritsky H (1952) The collapse or growth of a spherical bubble or cavity in a viscous fluid. In: Sternberg E (ed) Proceedings of the first US national congress on applied mechanics. ASME, New York, pp 813–821
87. Keller JB, Miksis M (1980) Bubble oscillations of large amplitude. J Acoust Soc Am 68:628–633
88. Trilling L (1952) The collapse and rebound of a gas bubble. J Appl Phys 23:14–17
89. Herring C (1941) Theory of the pulsations of the gas bubble produced by an underwater explosion. Washington p 236
90. Gilmore FR (1952) The growth or collapse of a spherical bubble in a viscous compressible liquid. California Institute of Technology. Hydrodynamics Laboratory, Pasadena, p 26
91. Lezzi A, Prosperetti A (1987) Bubble dynamics in a compressible liquid. 2. 2nd-order theory. J Fluid Mech 185:289–321
92. Prosperetti A, Lezzi A (1986) Bubble dynamics in a compressible liquid. 1. 1st order theory. J Fluid Mech 168:457–478
93. Prosperetti A (1987) The equation of bubble dynamics in a compressible liquid. Phys Fluids 30:3626–3628
94. Brenner MP et al (2002) Single-bubble sonoluminescence. Rev Mod Phys 74:425–484
95. Doinikov AA, Bouakaz A (2011) Review of shell models for contrast agent microbubbles. IEEE Trans Ultrason Ferroelectr Freq Control 58:981–993
96. Faez T et al (2013) 20 years of ultrasound contrast agent modeling. IEEE Trans Ultrason Ferroelectr Freq Control 60:7–20
97. Roy RA et al. (1990) Cavitation produced by short pulses of ultrasound. In: Frontiers of nonlinear acoustics: proceedings of 12th international symposium of nonlinear acoustics. London, pp 476–481
98. deJong N et al (1994) Higher harmonics of vibrating gas-filled microspheres 2. Meas Ultrason 32:455–459
99. deJong N et al (1994) Higher harmonics of vibrating gas-filled microspheres. 1. Simul Ultrason 32:447–453
100. deJong N, Hoff L (1993) Ultrasound scattering properties of albunex microspheres. Ultrasonics 31:175–181
101. deJong N et al (1992) Absorption and scatter of encapsulated gas filled microspheres—theoretical considerations and some measurements. Ultrasonics 30:95–103
102. Church CC (1995) The effects of an elastic solid-surface layer on the radial pulsations of gas-bubbles. J Acoust Soc Am 97:1510–1521
103. Hoff L et al (2000) Oscillations of polymeric microbubbles: effect of the encapsulating shell. J Acoust Soc Am 107:2272–2280
104. Morgan KE et al (2000) Experimental and theoretical evaluation of microbubble behavior: effect of transmitted phase and bubble size. IEEE Trans Ultrason Ferroelectr Freq Control 47:1494–1509
105. Glazman RE (1983) Effects of adsorbed films on gas bubble radial oscillations. J Acoust Soc Am 74:980–986
106. Khismatullin DB, Nadim A (2002) Radial oscillations of encapsulated microbubbles in viscoelastic liquids. Phys Fluids 14:3534–3557
107. Allen JS et al (2002) Dynamics of therapeutic ultrasound contrast agents. Ultrasound Med Biol 28:805–816
108. Allen JS, Rashid MM (2004) Dynamics of a hyperelastic gas-filled spherical shell in a viscous fluid. J Appl Mech Trans ASME 71:195–200
109. Chatterjee D, Sarkar K (2003) A Newtonian rheological model for the interface of microbubble contrast agents. Ultrasound Med Biol 29:1749–1757
110. Sarkar K et al (2005) Characterization of ultrasound contrast microbubbles using in vitro experiments and viscous and viscoelastic interface models for encapsulation. J Acoust Soc Am 118:539–550
111. Paul S et al (2010) Material characterization of the encapsulation of an ultrasound contrast microbubble and its subharmonic response: Strain-softening interfacial elasticity model. J Acoust Soc Am 127:3846–3857
112. Paul S et al (2013) Determination of the interfacial rheological properties of a poly(DL-lactic acid)-encapsulated contrast agent

using in vitro attenuation and scattering. Ultrasound Med Biol 39(7):1277–1291
113. Marmottant P et al (2005) A model for large amplitude oscillations of coated bubbles accounting for buckling and rupture. J Acoust Soc Am 118:3499–3505
114. Doinikov AA, Dayton PA (2007) Maxwell rheological model for lipid-shelled ultrasound microbubble contrast agents. J Acoust Soc Am 121:3331–3340
115. Tsiglifis K, Pelekasis NA (2008) Nonlinear radial oscillations of encapsulated microbubbles subject to ultrasound: the effect of membrane constitutive law. J Acoust Soc Am 123:4059–4070
116. Stride E (2008) The influence of surface adsorption on microbubble dynamics. Philos Trans R Soc Math Phys Eng Sci 366:2103–2115
117. Doinikov AA et al (2009) Modeling of nonlinear viscous stress in encapsulating shells of lipid-coated contrast agent microbubbles. Ultrasonics 49:269–275
118. Marmottant P et al (2011) Buckling resistance of solid shell bubbles under ultrasound. J Acoust Soc Am 129:1231–1239
119. Li Q et al (2013) Modeling complicated rheological behaviors in encapsulating shells of lipid-coated microbubbles accounting for nonlinear changes of both shell viscosity and elasticity. Phys Med Biol 58:985–998
120. Katiyar A, Sarkar K (2011) Excitation threshold for subharmonic generation from contrast microbubbles. J Acoust Soc Am 130:3137–3147
121. Prosperetti A (1977) Thermal effects and damping mechanisms in the forced radial oscillations of gas bubbles in liquids. J Acoust Soc Am 61:17–27
122. Ainslie MA, Leighton TG (2011) Review of scattering and extinction cross-sections, damping factors, and resonance frequencies of a spherical gas bubble. J Acoust Soc Am 130:3184–3208
123. Prosperetti A (1991) The thermal behaviour of oscillating gas bubbles. J Fluid Mech 222:587–616
124. van der Meer SM et al (2007) Microbubble spectroscopy of ultrasound contrast agents. J Acoust Soc Am 121:648–656
125. Katiyar A, Sarkar K (2012) Effects of encapsulation damping on the excitation threshold for subharmonic generation from contrast microbubbles. J Acoust Soc Am 132:3576–3585
126. Sijl J et al (2010) Subharmonic behavior of phospholipid-coated ultrasound contrast agent microbubbles. J Acoust Soc Am 128:3239–3252
127. Prosperetti A (2013) A general derivation of the subharmonic threshold for non-linear bubble oscillations. J Acoust Soc Am 133:3719–3726
128. Chang PH et al (1995) Second-harmonic imaging and harmonic Doppler measurements with Albunex(R). IEEE Trans Ultrason Ferroelectr Freq Control 42:1020–1027
129. Hoff L (2001) Acoustic characterization of contrast agents for medical ultrasound imaging. Kluwer Academic, Norwell
130. Gorce JM et al (2000) Influence of bubble size distribution on the echogenicity of ultrasound contrast agents—a study of SonoVue (TM). Investig Radiol 35:661–671
131. Tu J et al (2009) Estimating the shell parameters of SonoVue (R) microbubbles using light scattering. J Acoust Soc Am 126:2954–2962
132. Tu J et al (2011) Microbubble sizing and shell characterization using flow cytometry. IEEE Trans Ultrason Ferroelectr Freq Control 58:955–963
133. Morgan K et al (1998) The effect of the phase of transmission on contrast agent echoes. IEEE Trans Ultrason Ferroelectr Freq Control 45:872–875
134. Dayton PA et al (1999) Optical and acoustical observations of the effects of ultrasound on contrast agents. IEEE Trans Ultrason Ferroelectr Freq Control 46:220–232
135. de Jong N et al (2000) Optical imaging of contrast agent microbubbles in an ultrasound field with a 100-MHz camera. Ultrasound Med Biol 26:487–492
136. Sboros V et al (2006) Nanointerrogation of ultrasonic contrast agent microbubbles using atomic force microscopy. Ultrasound Med Biol 32:579–585
137. Kooiman K et al (2010) Lipid distribution and viscosity of coated microbubbles. IEEE in Ultrason Symp (IUS) 2010:900–903
138. Hosny NA et al (2013) Mapping microbubble viscosity using fluorescence lifetime imaging of molecular rotors. Proc Natl Acad Sci 10:9225–9230
139. Hughes MS et al (2000) Broadband time-domain reflectometry measurement of attenuation and phase velocity in highly attenuating suspensions with application to the ultrasound contrast medium Albunex (R). J Acoust Soc Am 108:813–820
140. Grishenkov D et al (2009) Characterization of acoustic properties of Pva-shelled ultrasound contrast agents: linear properties (part I). Ultrasound Med Biol 35:1127–1138
141. Overvelde M et al (2010) Nonlinear shell behavior of phospholipid-coated microbubbles. Ultrasound Med Biol 36:2080–2092
142. Brennen CE (1995) Cavitation and bubble dynamics. Oxford University Press, Oxford
143. Eisenbrey JR et al (2008) Effect of molecular weight and end capping on poly(lactic-co-glycolic acid) ultrasound contrast agents. Polym Eng Sci 48:1785–1792
144. El-Sherif DM, Wheatley MA (2003) Development of a novel method for synthesis of a polymeric ultrasound contrast agent. J Biomed Mater Res Part A 66A:347–355
145. Forsberg F et al (2004) Effect of shell type on the in vivo backscatter from polymer-encapsulated microbubbles. Ultrasound Med Biol 30:1281–1287
146. Sirsi SR et al (2009) Formulation of polylactide-co-glycolic acid nanospheres for encapsulation and sustained release of poly(ethylene imine)-poly(ethylene glycol) copolymers complexed to oligonucleotides. J Nanobiotechnol 7:1
147. Wheatley MA et al (2006) Comparison of in vitro and in vivo acoustic response of a novel 50: 50 PLGA contrast agent. Ultrasonics 44:360–367
148. El-Sherif D (2003) Development of novel PLGA contrast agents for use as ultrasound targeted drug delivery vehicles. Drexel University Philadelphia, PhD
149. Shi WT, Forsberg F (2000) Ultrasonic characterization of the nonlinear properties of contrast microbubbles. Ultrasound Med Biol 26:93–104
150. Preston AT et al (2007) A reduced-order model of diffusive effects on the dynamics of bubbles. Phys Fluids 19:123302
151. Nigmatulin RI et al (1981) Dynamics, heat and mass-transfer of vapour-gas bubbles in a liquid. Int J Heat Mass Transf 24:1033–1044
152. Shankar PM et al (1998) Advantages of subharmonic over second harmonic backscatter for contrast-to-tissue echo enhancement. Ultrasound Med Biol 24:395–399
153. Forsberg F et al (2000) Subharmonic imaging of contrast agents. Ultrasonics 38:93–98
154. Bhagavatheeshwaran G et al (2004) Subharmonic signal generation from contrast agents in simulated neovessels. Ultrasound Med Biol 30:199–203
155. Krishna PD et al (1999) Subharmonic generation from ultrasonic contrast agents. Phys Med Biol 44:681–694
156. Shankar PM et al (1999) Subharmonic backscattering from ultrasound contrast agents. J Acoust Soc Am 106:2104–2110
157. Shi WT et al (1999) Subharmonic imaging with microbubble contrast agents: Initial results. Ultrason Imaging 21:79–94

158. Faez T et al (2011) Characterizing the subharmonic response of phospholipid-coated microbubbles for carotid imaging. Ultrasound Med Biol 37:958–970
159. Goertz DE et al (2007) Subharmonic contrast intravascular ultrasound for vasa vasorum imaging. Ultrasound Med Biol 33:1859–1872
160. Frijlink ME et al (2006) Intravascular ultrasound tissue harmonic imaging: a simulation study. Ultrasonics 44:E185–E188
161. Goertz DE et al (2006) Contrast harmonic intravascular ultrasound—a feasibility study for vasa vasorum imaging. Investig Radiol 41:631–638
162. Shekhar H, Doyley MM (2012) Improving the sensitivity of high-frequency subharmonic imaging with coded excitation: a feasibility study. Med Phys 39:2049–2060
163. Shi WT et al (1999) Pressure dependence of subharmonic signals from contrast microbubbles. Ultrasound Med Biol 25:275–283
164. Shi WT et al (1999) Noninvasive pressure estimation with US microbubble contrast agents. Radiology 213P:101–101
165. Adam D et al (2005) On the relationship between encapsulated ultrasound contrast agent and pressure. Ultrasound Med Biol 31:673–686
166. Leodore L et al (2007) Subharmonic contrast microbubble signals for noninvasive pressure estimation: an in vitro study. Circulation 116:646–646
167. Leodore L et al (2007) In vitro pressure estimation obtained from subharmonic contrast microbubble signals. IEEE Ultrason Symp: 2207–2210
168. Leodore LM et al (2008) Implementation of noninvasive subharmonic pressure estimation on a commercial ultrasound scanner. Circulation 118:S1039–S1039
169. Frinking PJA et al (2010) Subharmonic scattering of phospholipid-shell microbubbles at low acoustic pressure amplitudes. IEEE Trans Ultrason Ferroelectr Freq Control 57:1762
170. Dave JK et al (2011) Noninvasive estimation of dynamic pressures in vitro and in vivo using the subharmonic response from microbubbles. IEEE Trans Ultrason Ferroelectr Freq Control 58:2056–2066
171. Dave JK et al (2012) Investigating the efficacy of subharmonic aided pressure estimation for portal vein pressures and portal hypertension monitoring. Ultrasound Med Biol 38:1784–1798
172. Dave JK et al (2012) Subharmonic microbubble emissions for noninvasively tracking right ventricular pressures. Am J Physiol Heart Circ Physiol 303:H126–H132
173. Dave JK et al (2012) Noninvasive LV pressure estimation using subharmonic emissions from microbubbles. JACC Cardiovasc Imaging 5:87–92
174. Halldorsdottir VG et al (2011) Subharmonic contrast microbubble signals for noninvasive pressure estimation under static and dynamic flow conditions. Ultrason Imaging 33:153–164
175. Katiyar A et al (2011) Modeling subharmonic response from contrast microbubbles as a function of ambient static pressure. J Acoust Soc Am 129:2325–2335
176. Chetty K et al (2008) High-speed optical observations and simulation results of SonoVue microbubbles at low-pressure insonation. IEEE Trans Ultrason Ferroelectr Freq Control 55:1333–1342
177. Chin CT et al (2003) Brandaris 128: a digital 25 million frames per second camera with 128 highly sensitive frames. Rev Sci Instrum 74:5026–5034
178. Sun Y et al (2005) High-frequency dynamics of ultrasound contrast agents. IEEE Trans Ultrason Ferroelectr Freq Control 52:1981–1991
179. Caskey CF et al (2007) Direct observations of ultrasound microbubble contrast agent interaction with the microvessel wall. J Acoust Soc Am 122:1191–1200
180. Sun Y et al (2006) Observation of contrast agent response to chirp insonation with a simultaneous optical-acoustical system. IEEE Trans Ultrason Ferroelectr Freq Control 53:1130–1137
181. Guan JF, Matula TJ (2004) Using light scattering to measure the response of individual ultrasound contrast microbubbles subjected to pulsed ultrasound in vitro. J Acoust Soc Am 116:2832–2842
182. Renaud G et al (2012) An acoustical camera for in vitro characterization of contrast agent microbubble vibrations. Appl Phys Lett 100:101911
183. Postema M et al (2004) Ultrasound-induced encapsulated microbubble phenomena. Ultrasound Med Biol 30:827–840
184. Hsu MJ et al (2011) Characterization of individual ultrasound microbubble dynamics with a light-scattering system. J Biomed Opt 16(6):067002
185. De Jong N et al (2007) Compression-only behavior of phospholipid-coated contrast bubbles. Ultrasound Med Biol 33:653–656
186. Vos HJ et al (2007) Orthogonal observations of vibrating microbubbles. IEEE Symp Ultrason 765–768
187. Emmer M et al (2007) The onset of microbubble vibration. Ultrasound Med Biol 33:941–949
188. Dollet B et al (2008) Nonspherical oscillations of ultrasound contrast agent microbubbles. Ultrasound Med Biol 34:1465–1473
189. de Jong N et al (2009) Ultrasonic characterization of ultrasound contrast agents. Med Biol Eng Comput 47:861–873
190. Vos HJ et al (2008) Nonspherical vibrations of microbubbles in contact with a wall—a pilot study at low mechanical index. Ultrasound Med Biol 34:685–688
191. Zhao SK et al (2005) Asymmetric oscillation of adherent targeted ultrasound contrast agents. Appl Phys Lett 87:134103
192. Versluis M Nonlinear behavior of ultrasound contrast agent microbubbles and why shell buckling matters
193. Sijl J et al (2008) Acoustic characterization of single ultrasound contrast agent microbubbles. J Acoust Soc Am 124:4091–4097
194. Sboros V et al (2005) Absolute measurement of ultrasonic backscatter from single microbubbles. Ultrasound Med Biol 31:1063–1072
195. Sboros V et al (2007) Acoustic Rayleigh scattering at individual micron-sized bubbles. Appl Phys Lett 90:123902
196. Klibanov AL et al (2004) Detection of individual microbubbles of ultrasound contrast agents: imaging of free-floating and targeted bubbles. Investig Radiol 39:187–195
197. Klibanov AL et al (2002) Detection of individual microbubbles of an ultrasound contrast agent: fundamental and pulse inversion imaging. Acad Radiol 9:S279–S281
198. Sboros V (2010) A review of single microbubble acoustics, pp 710–714
199. Thomas DH et al (2009) Acoustic detection of microbubble resonance. Appl Phys Lett 94:243902–243903
200. Sijl J et al (2011) Combined optical and acoustical detection of single microbubble dynamics. J Acoust Soc Am 130:3271–3281
201. Thomas DH et al (2009) Single microbubble response using pulse sequences: initial results. Ultrasound Med Biol 35:112–119
202. Guidi F et al (2010) Microbubble characterization through acoustically induced deflation. IEEE Trans Ultrason Ferroelectr Freq Control 57:193–202
203. Chitnis PV et al (2013) Influence of shell properties on high-frequency ultrasound imaging and drug delivery using polymer-shelled microbubbles. IEEE Trans Ultrason Ferroelectr Freq Control 60:53–64
204. Chitnis PV et al (2011) Rupture threshold characterization of polymer-shelled ultrasound contrast agents subjected to static overpressure. J Appl Phys 109:084906
205. Ketterling JA et al (2007) Excitation of polymer-shelled contrast agents with high-frequency ultrasound. J Acoust Soc Am 121:El48–El53

206. Gong Y (2013) Acoustic characterization of ultrasound contrast agents with lipid-coated monodisperse microbubble, 3529049 Ph.D. Boston University, Massachusetts
207. Pancholi KP et al (2008) Novel methods for preparing phospholipid coated microbubbles. Eur Biophys J Biophys Lett 37:515–520
208. Stride E, Edirisinghe M (2009) Novel preparation techniques for controlling microbubble uniformity: a comparison. Med Biol Eng Comput 47:883–892
209. Talu E et al (2008) Maintaining monodispersity in a microbubble population formed by flow-focusing. Langmuir 24:1745–1749
210. Hettiarachchi K et al (2006) Formulation of monodisperse contrast agents in microfluidic systems for ultrasonic imaging, in microtechnologies in medicine and biology. International Conference on 2006:230–232
211. Gong Y et al (2010) Relationship between size and frequency dependent attenuation of monodisperse populations of lipid coated microbubbles. Bubble Sci Eng Technol 2:41–47
212. Gong Y et al (2010) Pressure-dependent resonance frequency for lipid-coated microbubbles at low acoustic pressures. IEEE Ultrason Symp (IUS) 2010:1932–1935
213. Demos SM et al (1999) In vivo targeting of acoustically reflective liposomes for intravascular and transvascular ultrasonic enhancement. J Am Coll Cardiol 33:867–875
214. Buchanan KD et al (2008) Echogenic liposome compositions for increased retention of ultrasound reflectivity at physiologic temperature. J Pharm Sci 97:2242–2249
215. Coussios CC et al (2004) In vitro characterization of liposomes and optison (R) by acoustic scattering at 3.5 MHz. Ultrasound Med Biol 30:181–190
216. Lu S-C et al (2007) Echogenic liposomes in high-frequency ultrasound imaging. IEEE Ultrason Symp 2203–2206
217. Smith DAB et al (2007) Destruction thresholds of echogenic liposomes with clinical diagnostic ultrasound. Ultrasound Med Biol 33:797–809
218. Radhakrishnan K et al (2012) Stability of echogenic liposomes as a blood pool ultrasound contrast agent in a physiologic flow phantom. Ultrasound Med Biol 38:1970–1981
219. Haworth KJ et al (2012) Passive imaging with pulsed ultrasound insonations. J Acoust Soc Am 132:544–553
220. Sax N, Kodama T (2013) Optimization of acoustic liposomes for improved in vitro and in vivo stability. Pharm Res 30:218–224
221. Laing ST, McPherson DD (2009) Cardiovascular therapeutic uses of targeted ultrasound contrast agents. Cardiovasc Res 83:626–635
222. Buchanan KD et al (2010) Encapsulation of NF-kappa B decoy oligonucleotides within echogenic liposomes and ultrasound-triggered release. J Controlled Release 141:193–198
223. Shaw GJ et al (2009) Ultrasound-enhanced thrombolysis with tPA-loaded echogenic liposomes. Thrombosis Res 124:306–310
224. Herbst SM et al (2010) Delivery of stem cells to porcine arterial wall with echogenic liposomes conjugated to antibodies against CD34 and intercellular adhesion molecule-1. Mol Pharm 7:3–11
225. Hamilton A et al (2002) A physiologic flow chamber model to define intravascular ultrasound enhancement of fibrin using echogenic liposomes. Investig Radiol 37:215–221
226. Demos SM et al (1997) In vitro targeting of antibody-conjugated echogenic liposomes for site-specific ultrasonic image enhancement. J Pharm Sci 86:167–171
227. Kim H et al (2010) In vivo volumetric intravascular ultrasound visualization of early/inflammatory arterial atheroma using targeted echogenic immunoliposomes. Investig Radiol 45:685–691. doi:10.1097/RLI.0b013e3181ee5bdd
228. Hamilton A et al (2002) Left ventricular thrombus enhancement after intravenous injection of echogenic immunoliposomes—studies in a new experimental model. Circulation 105:2772–2778
229. Tiukinhoy SD et al (2000) Development of echogenic, plasmid-incorporated, tissue-targeted cationic liposomes that can be used for directed gene delivery. Investig Radiol 35:732–738
230. Tiukinhoy SD et al (2004) Novel echogenic drug-immunoliposomes for drug delivery. Investig Radiol 39:104–110
231. Huang SL et al (2007) Multi-functional echogenic liposomes for image-guided and ultrasound-controlled PPAR agonist delivery. J Am Coll Cardiol 49:365a–365a
232. Laing ST et al (2011) Ultrasound-enhanced thrombolytic effect of tissue plasminogen activator-loaded echogenic liposomes in an in vivo rabbit aorta thrombus model-brief report. Arterioscler Thromb Vasc Biol 31:1357–1359
233. Tiukinhoy-Laing SD et al (2007) Fibrin targeting of tissue plasminogen activator-loaded echogenic liposomes. J Drug Targ 15:109–114
234. Tiukinhoy-Laing SD et al (2007) Ultrasound-facilitated thrombolysis using tissue-plasminogen activator-loaded echogenic liposomes. Thromb Res 119:777–784
235. Kee P et al (2007) Synthesis and acoustic characterization of a novel ultrasound controlled drug delivery system based on echogenic liposomes. J Am Coll Cardiol 49:120a–120a
236. Moody MR et al (2008) Bioactive gas/drug co-encapsulation and release improve attenuation of intimal hyperplasmia following acute arterial injury. Circulation 118:S573–S573
237. Kopechek JA et al (2013) The impact of bubbles on measurement of drug release from echogenic liposomes. Ultrason Sonochem 20:1121–1130
238. Britton GL et al (2010) In vivo therapeutic gas delivery for neuroprotection with echogenic liposomes. Circulation 122:1578–1587
239. Huang SL et al (2009) Nitric oxide-loaded echogenic liposomes for nitric oxide delivery and inhibition of intimal hyperplasia. J Am Coll Cardiol 54:652–659
240. Huang SL et al (2007) Nitric oxide loaded echogenic liposomes inhibit intimal hyperplasia in an acute arterial injury model. Circulation 116:294–294
241. Britton G et al (2009) Nitric oxide loaded echogenic liposomes for ultrasound controlled nitric oxide delivery and regulation of artery diameter. Stroke 40:E119–E120
242. Evjen TJ et al (2010) Distearoylphosphatidylethanolamine-based liposomes for ultrasound-mediated drug delivery. Eur J Pharm Biopharm 75:327–333
243. Lin HY, Thomas JL (2004) Factors affecting responsivity of unilamellar liposomes to 20 kHz ultrasound. Langmuir ACS J Surf Colloids 20:6100–6106
244. Sarkar N et al (2007) Matrix metalloproteinase-assisted triggered release of liposomal contents. Bioconj Chem 19:57–64
245. Chandra B et al (2006) Formulation of photocleavable liposomes and the mechanism of their content release. Org Biomol Chem 4:1730–1740
246. Kopechek JA et al (2010) Calibration of the 1-Mhz sonitron ultrasound system. Ultrasound Med Biol 36:1762–1766
247. Laing S et al (2008) Doppler ultrasound enhances the thrombolytic activity of tissue plasminogen activator-loaded echogenic liposomes in vivo. Circulation 118:S643–S643
248. Bauvois B (2012) New facets of matrix metalloproteinases MMP-2 and MMP-9 as cell surface transducers: outside-in signaling and relationship to tumor progression. Biochim Et Biophys Acta Rev Cancer 1825:29–36
249. Pytliak M et al (2012) Matrix metalloproteinases and their role in oncogenesis: a review. Onkologie 35:49–53
250. Bloomston M et al (2002) Matrix metalloproteinases and their role in pancreatic cancer: a review of preclinical studies and clinical trials. Ann Surg Oncol 9:668–674
251. Duffy MJ, McCarthy K (1998) Matrix metalloproteinases in cancer: prognostic markers and targets for therapy (review). Int J Oncol 12:1343–1348

252. Jones CB et al (2003) Matrix metalloproteinases: a review of their structure and role in acute coronary syndrome. Cardiovasc Res 59:812–823
253. Hobeika MJ et al (2007) Matrix metalloproteinases in peripheral vascular disease. J Vasc Surg 45:849–857
254. West KR, Otto S (2005) Reversible covalent chemistry in drug delivery. Curr Drug Discov Technol 2:123–160
255. Goldenbogen B et al (2011) Reduction-sensitive liposomes from a multifunctional lipid conjugate and natural phospholipids: reduction and release kinetics and cellular uptake. Langmuir 27:10820–10829
256. Cho H et al (2012) Redox-sensitive polymeric nanoparticles for drug delivery. Chem Commun (Camb)
257. Wen H et al (2012) Engineered redox-responsive PEG detachment mechanism in PEGylated nano-graphene oxide for intracellular drug delivery. Small 8:760–769
258. Stride E, Saffari N (2005) Investigating the significance of multiple scattering in ultrasound contrast agent particle populations. IEEE Trans Ultrason Ferroelectr Freq Control 52:2332–2345
259. Qamar A et al (2013) Dynamics of micro-bubble sonication inside a phantom vessel. Appl Phys Lett 102:013702–013705
260. Garbin V et al (2007) Changes in microbubble dynamics near a boundary revealed by combined optical micromanipulation and high-speed imaging. Appl Phys Lett 90:114103–114103
261. Doinikov AA et al (2011) Acoustic scattering from a contrast agent microbubble near an elastic wall of finite thickness. Phys Med Biol 56:6951–6967
262. Loughran J et al (2012) Modeling non-spherical oscillations and stability of acoustically driven shelled microbubbles. J Acoust Soc Am 131:4349–4357
263. Pauzin MC et al (2007) Development of a finite element model of ultrasound contrast agent. IEEE Ultrason Symp 1989–1992
264. Maul TM et al (2010) Optimization of ultrasound contrast agents with computational models to improve selection of ligands and binding strength. Biotechnol Bioeng 107:854–864